Development on Impedance Measurement System For Electrochemical Impedance Spectroscopy

by

Jiajun Li

A thesis submitted in partial fulfillment of the requirements for the degree of

Master of Science

in

Microsystems and Nanodevices

Department of Electrical and Computer Engineering

University of Alberta

Abstract

Electrochemical impedance spectroscopy (EIS) has been used in various applications, such as metal corrosion monitoring. However, many conventional corrosion monitoring setups are bulky and inconvenient for in-situ testing. Reducing the size of the whole corrosion monitoring system is one of the purposes of this thesis. We utilized EIS to design an impedance measurement system, capable of performing in-situ EIS analysis. Experiments verified the sensor's accuracy, and the results showed that the sensor performed similarly to a bench-top EIS machine when we tested on circuit models. Furthermore, we used the proposed system to monitor a metal corrosion experiment and performed EIS. The result showed that the proposed system is able to obtain the sample's impedance spectroscopy, which could help researchers test its corrosion severity on a metallic sample in-situ. Compared to other bulky conventional setups, our device eliminates the design complexity while still showing insights into the corrosion reaction.

Also, we briefly introduce the ongoing work: the impedance measurement system for the COVID-19 project. The purpose of this work is to help with the EIS analysis with the customized measurement system. Compared to the corrosion one, the new system has several changes. We introduce these changes and show the testing result.

To my parents

Stand up straight with your shoulders back.

– Jordan B. Peterson

Acknowledgements

Foremost, I would like to sincerely acknowledge my supervisor, Prof.Jie Chen, for giving me the opportunity to work in the BINARY research group at the Department of Electrical and Computer Engineering, University of Alberta. Prof.Chen provided me with a lot of research opportunities and helped me along with my study. When I encounter difficulties and confusion in my scientific research, Prof.Chen can always help me find solutions to problems. The ECE750 taught by Prof.Chen gave me a lot of professional knowledge and research methodologies on biomedical engineering and nanotechnology. Thank Prof.Chen for his help and support with my study!

Meanwhile, during my study at the University of Alberta, it was an honor for me to work with many talented researchers: Dr.Xiaoxue Jiang, Xuanjie Ye, Kaining Mao, Pedro Duarte Riveros, Lukas Menze, Tianxiang Jiang, Shuren Wang, etc. Also, I would like to thank the CEO of Fourien Inc, Dr.Faheem Khan, for providing help for the research projects. Working and studying with these individuals is such an enjoyable journey!

This thesis was completed during the COVID-19 pandemic. For many people, these days are tough. I want to thank healthcare and essential workers at this time especially. Their hard work is the guarantee that we can return to everyday life.

Finally, I would like to express my gratitude to my parents. Their love, guide, and support are essential for me in every steps of my life.

Contents

List of Tables

List of Figures

Chapter 1

Introduction

This chapter gives the readers the background information of this study. Firstly, the metal corrosion phenomenon is illustrated. After that, we introduced one of the methods of montoring metal corrosion in lab testing, EIS (Electrochemical Impedance Spectroscopy) analysis. Then comes different kinds of portable EIS devices that appeared in the reported literature. The outline of the whole thesis locates at the end of this chapter.

1.1 Metal Corrosion Phenomenon

Metal materials are widely used in many industries. It is easy to find items made of metal in our daily life. The reasons metal materials have been so extensively used are their abundant resources on earth and excellent performance in various areas. However, most metal materials will encounter a problem, that is, metal corrosion[1]–[3]. As a result of metal corrosion, the structure of the metal material starts to degenerate. Phenomenon such as metal rusting occurs. As a result of metal corrosion, the structure of the metal material starts to degenerate. As the corrosion develops even further, the metal structure could weaken, leading to economic losses and safety issues[4]. Also, the product of some metal corrosion reaction causes serious pollution problems[5].

Metal corrosion often occurs when a piece of metal exposed to the elec-

trolyte solution[6]. For example, when immersed in NaCl solution or sea salt aerosol, metal could occur at the surface of the metal sample[7], [8]. In this process, atoms on the surface of the metal sample become metal ions by losing electrons. That is to say, the metal has undergone an oxidation reaction [9], [10].

Generally speaking, metal corrosion is generally divided into two mechanisms: chemical corrosion and electrochemical corrosion[11]. In the non-electrolyte solution or dry gas, the metal material directly reacts with the non-electrolyte solution. In this process, metal materials are consumed and suffer certain damages. The reaction between active metals and strong acids can be regarded as chemical corrosion of metals[11]. For example, the displacement reaction between iron and hydrochloric acid[12], [13]. It is important that no current is generated during the chemical corrosion process[14].

For the electrochemical corrosion of metals, first of all, this reaction occurs between the metal and the electrolyte solution. This reaction can occur even in electrolyte solution aerosols[7]. When the metal and the electrolyte solution come into contact, an electrochemical reaction will occur at the interface between the two[15], [5]. In this case, the metal and electrolyte solution will form a corrosive galvanic cell[16]. Corrosion current will be generated. The electrochemical reaction here is a redox reaction, in which the more active metal will lose electrons and form metal ions[9], [10]. As the reaction progresses, on a microscopic level, a large number of metal atoms become ions. Macroscopically, the surface of the metal sample loses its luster, rusts, and the structure is damaged.These two different reaction mechanisms may occur simultaneously[17]. Besides, a series of factors such as humidity, temperature, and oxygen concentration in the environment, etc., will become the reasons that affect the corrosion reaction rate[1], [17]. Figure1.1 shows an example of the metal corrosion phenomenon on the chassis of a car. Metal rust appears

on the chassis, which indicated that those metal parts had been corroded.

Figure 1.1: Example of metal corrosion pheonmenon on the chassis of a car

The economic loss caused by metal corrosion can be as significant as 2%-4% of each country's gross domestic product (GDP)[1]. Such a large loss will make people alert. So people have found many ways to protect metal materials. Among these methods, the cathodic protection method is more useful. This is a measure of electrochemical protection of metals from corrosion. The metal with strong reducibility is used as the protective electrode, and the protected metal is connected to form a galvanic cell in the electrolyte solution. In a galvanic battery, the metal with strong reducibility will be used as the negative electrode to undergo oxidation reaction and be consumed in the reaction, and the protected metal will not be corroded as the positive electrode[15], [18], [19]. Another method to be introduced is to add coating to the metal. Obviously, by isolating metals and corrosive materials, the corrosion reaction will stop or slow down.

Just as important as the anti-corrosion protection measures for metals is the evaluation of the degree of metal corrosion and the surface protection

coating function[17]. Obviously, in order to systematically understand the phenomenon of metal corrosion, we need to conduct a quantitative analysis of this phenomenon.

1.2 Introduction to Electrochemical Impedance Spectroscopy(EIS) Analysis

In this section, Electrochemical Impedance Spectroscopy (EIS) will be introduced from these three different aspects. Firstly, we illustrate what the purpose, method and some application related to EIS. Next, we specifically focus on how to monitor metal corrosion with EIS. Lastly, some instruments that have been used to help perform EIS analysis, such as electrochemical station and impedance analyzer, will be briefly introduced.

1.2.1 Basic principle of EIS

The core idea of EIS is pretty simple. First, we need to measure the complex impedance spectra of the sample-under-test over a range of frequencies. Secondly, we fit the impedance data to an equivalent circuit[20]. After data fitting, the electrical behavior of the equivalent circuit is very close to the electrical behavior of the sample under test. In this case, we can analyse a particular property of the sample-under-test by analyzing a specific parameter in the equivalent circuit.

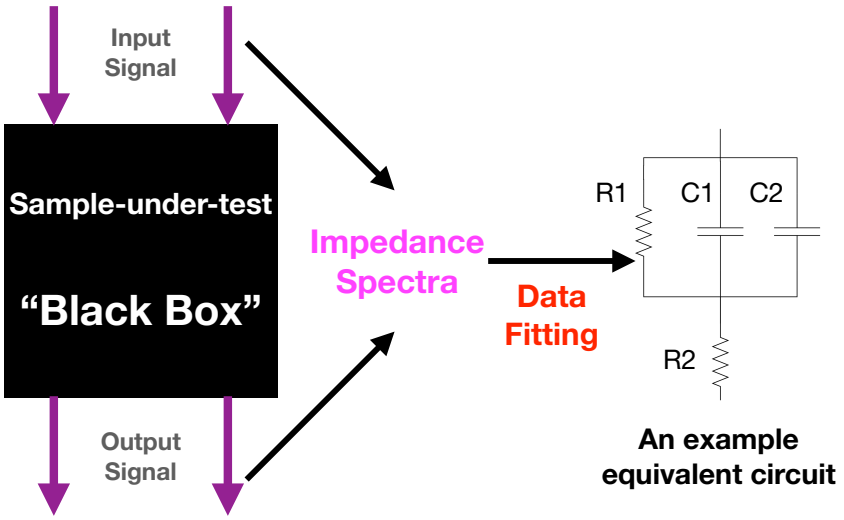

Figure 1.2: The process of EIS analysis.

We can elaborate on EIS analysis more straightforwardly. Figure 1.2 shows the process of an EIS analysis. On the left-hand side of the picture, the sample-under-test is regarded as a “Black Box,” which means that we do not know any detail of it, and it is the object we want to study. On the top of the “Black Box,” there is the input signal. The input signal can be a small-amplitude (mV amplitide level) disturbance or perturbation signal. The output signal from another end of the “Black Box” indicates the signal sensed at the output. Since there are no other input signals applied to the “Black Box” directly, the output signal is the response to the input signal. When the signal is going through the “Black Box”, there always will be some loss of the signal due to the impedance of the “Black Box.” Consequently, the output signal differs from the input signal. The two different signals are the critical information for us to conduct an EIS analysis, since we can compute the “Black Box” complex impedance by using the two signals. We can compute the complex impedance of the signal under the corresponding frequency for one pair of input and

output signals. Indeed, to get the impedance spectra, we need to perform a series of impedance measurements over a range of frequencies. Eventually, after completing many rounds of single-frequency impedance measurement, we should get the complex impedance spectra of the sample-under-test.

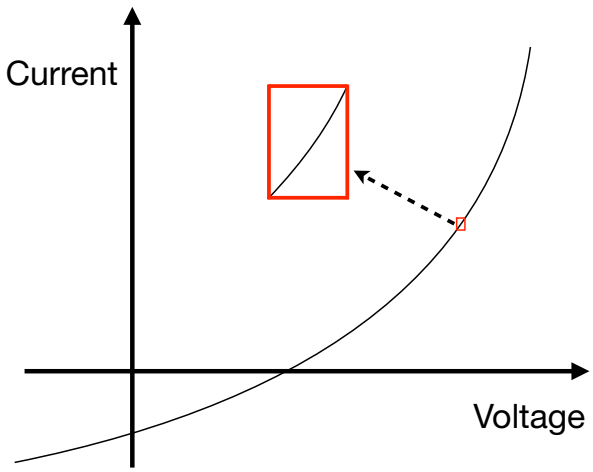

Figure 1.3: Pseudo-linearity in EIS analysis.

There is another critical concern of the EIS analysis that we need to be aware of. When we do EIS analysis on some given sample, the amplitude of the signal directly applied on the sample-under-test should be small enough. Figure 1.3 shows one possible I-V(Current-Voltage) relationship of a sample-under-test. It is obvious that the system behaves with a non-linear I-V characteristic. The analysis of a non-linear system is much more complex than simply analyzing a linear system. Even though we must admit the fact that the system is inherently linear no matter what kind of signal we use, we can use this "pseudo-linear" region. By limiting the signal amplitude, the signal operates in a tiny region as shown is the red box is figure 1.3. This approximate significantly reduced the computation effort of the EIS analysis. As a result, the analysis is easier for us[20].

However, this doesn't necessarily mean that the testing signal should be as small as possible. There are constraints when selecting the testing signal for the EIS analysis. In reality, all testing equipment suffers from the noise problem. The noise could be generated inside of the equipment or introduced from an external source. Once the amplitude is way too small, the low signal-to-noise ratio (SNR) will cause inaccuracy in the measurement result.

1.2.2 EIS in Corrosion Analysis

Electrochemical Impedance Spectroscopy (EIS) analysis is a very effective way to monitor metal corrosion. In the EIS analysis, the magnitude and phase of the sample's impedance at different frequencies are accurately measured. There are two main modes for monitoring the electro-chemical reactions of through EIS, i.e. the galvanostatic mode and the potentiostatic mode. Galvanostatic EIS analysis is mainly used in the development and research of large power devices such as batteries, where a current is fed into the system and the voltage signal was measured[21], [22]. For monitoring metal corrosion, potentiostatic EIS is the most commonly used method. At different frequencies in potentiostatic EIS, the required DC voltage across the sample is relatively stable. A small AC disturbance voltage signal is applied across the sample under test. Once the AC current through it and the AC voltage across it are known, the sample's complex impedance can be calculated[20], [8].

The method of using EIS to monitor corrosion phenomenon was developed in the late 20th century. In 1970, for the first time, Epelboin et al. interpred the inductive impedance of the metal-electrolyte interface by describing the phenomenon as a faradaic process[23]. In 1971, Epelboin et al. studied the corrosion of iron in the sulfuric aqueous medium, and they investigated the influence of 2-butyne 1,4-diol in the reaction with the method of impedance measurement and analysis[24]. One year later, in 1972, Epelboin et al. studied

the formation of sulphuric aqueous media still by the analysis on the complex impedance of the sample[25]. Most importantly, in [26], Epelboin et al. established the approach to determine the instant rate of metal corrosion.

Other scientists also contributed to the method of using EIS analysis to monitor metal corrosion. Mansfeld showed the EIS analysis as a new tool to investigate corrosion protection with coating, oxide layer and cathodic protection[27]. Jüttner, K presented the way to use EIS analysis to detect surface inhomogeneities in [28]. In this work, the corrosion process was analyzed based on the transfer function of the system. Also, the defects of the single and multi coating was discussed. Makar and Kruger investigated the rapidly solidified magnesium alloy corrosion phenomenon by measuring impedance and data fitting to a Randles circuit[27]. Currently, using such a method is still a popular way.

In order to measure impedance, we must first prepare impedance measurement samples. In the corrosion experiment, the corrosion cell often plays an important role in the experiment. For example, the EuroCell from GAMRY (Warminster, PA, USA) was used in the metal corrosion study due to the versatile experimental condition control[29], [30].

In order to simplify the corrosion cell model, we use a simple model to illustrate the corrosion cell. When a metal sample immerses in the electrolyte solution, reactions occur between the solution and the metal. Because of the reaction, there will be charges accumulate on the surface of the metal. For these accumulated charges, we can divide them into different layers. They are the stern layer and the diffuse layer (or the double layer)[31], [32]. In the EIS analysis, a small disturbance sine signal (input) is applied on the double layer from one end of the sample, forcing the charges to move towards or away from the metal. At another end, the response signal (output) is collected.The input and output signal are slightly different from each other

due to the energy loss when the signal passes through the sample. Comparing the input and the output sine waves, we can find information on the corrosion process. Specifically, we can find the complex impedance of the sample[20]. Figure 1.4 shows the charging and discharging of the double layer caused by the AC signal. To measure the sample's impedance, a two-electrode potentiostatic device is applied. A little disturbance signal is given to the sample, accounting for the charging and discharging effects of the corroding metal double layer. Of course, the instrument for EIS analysis of samples in a chemical laboratory is not as simple as a figure 1.4. In real experiments, the corrosion cell can help researchers better control the reaction conditions, so that the chemical reaction can be carried out under the conditions the researchers hope. But our interpretation makes the process in the corrosion cell more intuitive.

So far we have introduced the precautions for impedance measurement in EIS analysis. Then we will introduce the equivalent circuit we will use. This equivalent circuit allows us to better understand how the sample changes in the corrosion.The equivalent circuit we use is called Randles cell circuits, widely used in the EIS analysis[33]–[37]. We selected an equivalent circuit model as shown in Figure 1.5[38]–[40] R1 represents the resistance of the electrolytic solution[39] R2 and Q2 represent the electrochemical reaction layer, which Q2 is modeled using a constant phase model (CPE) and the paralleling resistance (R2) represents the metal/solution interface.

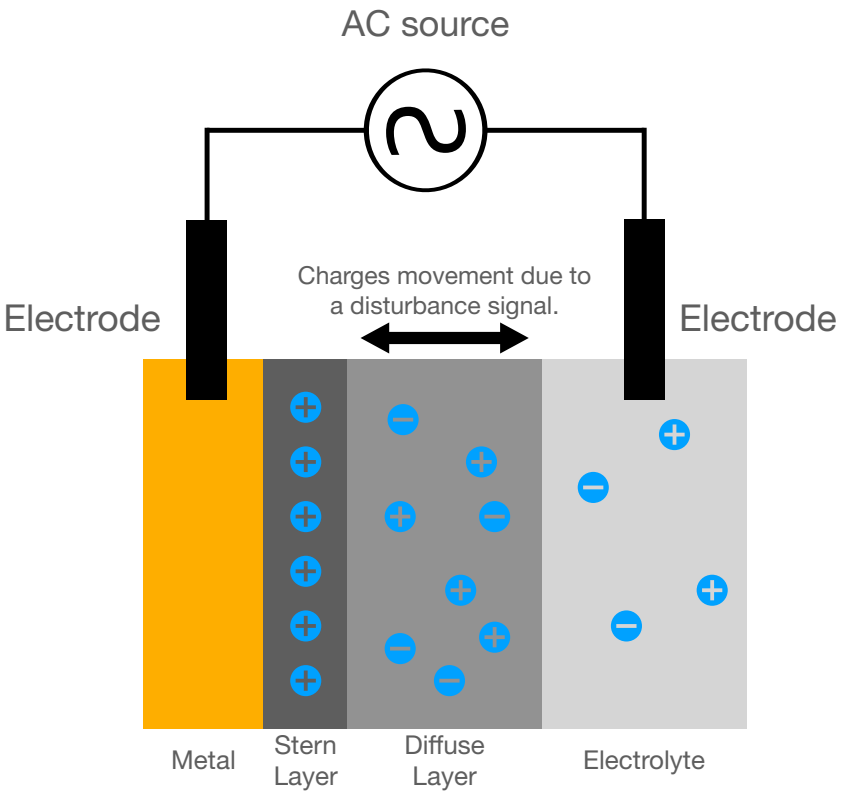

Figure 1.4: Charging and discharging of the double layer caused by the AC signal.

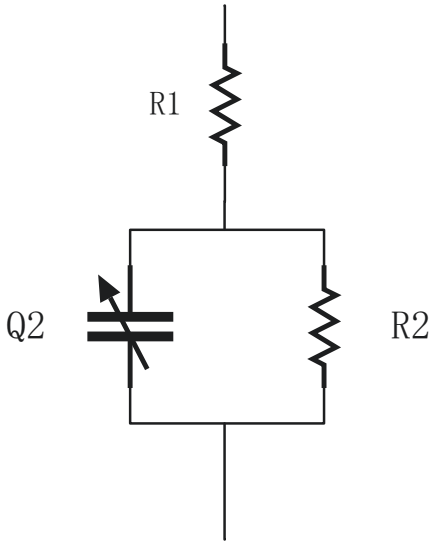

Figure 1.5: Randles cell circuit

$$\mathbf{Z} = \frac{\mathbf{1}}{\mathbf{Q}(\mathbf{j}\omega)^{\alpha}} \tag{1.1}$$

Equation 1.1 is the impedance expression of Q2 or CPE. In the equation, Q is the CPE value. CPE is an element that can model the behavior between a pure capacitor and a pure resistor. α is the exponential value that determines the CPE model's characteristic and takes the value between 0 and 1. When α=0, the CPE model is purely resistive. On the contrary, when α=1, it is strictly capacitive. In reality, the surface of the metal is rough. The purpose of using CPE is that we want to model the imperfection of the non-homogenous surface of the metal sample[41]. Also, if the surface is considered smooth, we can use a single capaitor to replace the CPE.

So far, we have introduced information about the use of EIS analysis for corrosion monitoring. Next, we will introduce the equipment needed for EIS analysis in the laboratory.

1.2.3 EIS Equipment Overview

When choosing impedance measurement equipment, there are several key features that we should be aware of.

- The working frequency range.
- The impedance magnitude result range.
- The accuracy of the equipment.
- The operation condition of the equipment.

Since most of the Impedance Analyzer follows the same approach of measurement: sending a sine signal and measure the response, the frequency of the sine signal is the working frequency of the device. Generally speaking, the equipment with wider frequency is better and more capable of a variety

of applications. The impedance magnitude range shows the capability of the impedance analyzer to measure different values of sample-under-test. Obviously, equipment with a broader range of measurement results is always desirable. For accuracy, it should be discussed under two conditions: the working frequency and the sample's impedance. The complex is a frequency-dependent parameter. That is to say, for the same sample-under-test, the impedance measurement results may differ from each other. In this case, the accuracy can be visualized to a 3-D graph. In the graph, one axis corresponds to the impedance, and another corresponds to the working frequency. Any given point in the graph maps to a certain accuracy calculation value corresponding to a pair of specific impedance and frequency. In order to get this picture, many measurements are necessary. Each measurement will get a point, and the collection of these points constitutes this 3D-graph. This graph is very important for us to choose an impedance analyzer. Because for a particular sample-under-test, we will have an estimate of the impedance magnitude. We need to choose an impedance analyzer with high accuracy within the estimated range.

Impedance measurement equipment is essential in the EIS analysis. Since there is much equipment available on the market that could conduct EIS analysis, it is impossible to introduce them all in this thesis. In this section introduces two different sets of commercial impedance measurement systems that could be used to conduct EIS analysis.

Firstly, we introduce the Impedance Analyzer from Zurich Imstrument.

Figure 1.6: MFIA 500 kHz / 5 MHz Impedance Analyzer by Zurich Instrument

Figure 1.6 shows the device from Zurich Instrument. It is an Impedance Analyzer as well as a precision LCR meter. The working frequency of the instrument could be as high as 5MHz and as low as 1mHz. The impedance result range is 1 mΩ to 1 TΩ. The device can a series of applications, including EIS analysis [42] and characterizing the property of a supercapacitor[43]. For accuracy, the equipment can reach 0.05% in a specific range of frequency and impedance. For phase, the accuracy could be as low as 2 mdeg[44]. Also, the equipment was used for semiconductor water evaluation[45].

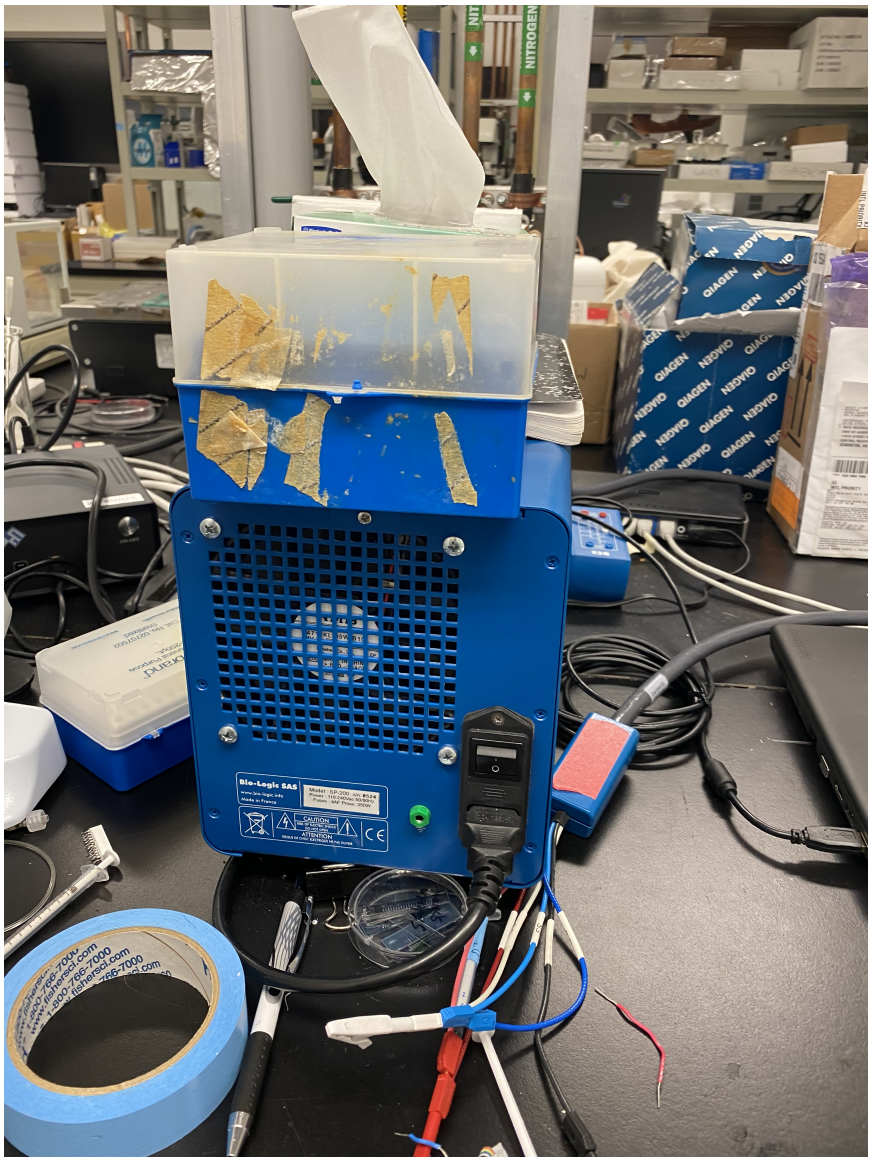

Figure 1.7: SP-200 Potentiostat by BioLogic

Figure 1.7 shows the SP-200 Potentiostat electrochemical workstation. The working frequency of the SP-200 ranges from 10 μHz to 7 MHz. The specification of the impedance measurement range is given as input current and current range. The input voltage range of the SP-200 is $\pm$10V and the input current range is 500 mA to 1 μA.(Could be 10 nA with gain)[46].

For the application of the SP-200, it is capable of doing corrosion analysis. Jegdić et al. investigated the pitting corrosion with a three-electrode

electrochemical cell by using the SP-200[47]. One of the feature of the Sp-200 is that it is a potentiostat. A potentiostat is essential in the electrochemical study[48]–[50].

1.3 Related Work

The purpose of this work is to minimize the size of the impedance measurement system. There has been a lot of work with the same aim. For these different works, most of them a dedicated to a specific application. These works inspired us to design the impedance measurement system for corrosion monitoring.

Yu et al. developed a n impedance detection circuit with a 3% error comparing to a LCR meter[51]. The device is designed to detect different biomolecules on a portable biosensor system. Jiang et al. have developed an EIS system that can be used as a bio-detection system[52]. The weight of the device is only 450g and the cost is about $45. The performance of the device is as follows. The frequency sweep is from 100 Hz to 500 kHz, the measurement range is 10 Ohm-100 kOhm, and the phase accuracy reaches 0.936°. In their experiment, the instrument carried out EIS analysis on eggs at different times during the heating process. Grassini et al. designed a miniaturized EIS system using Arduino, and the measured frequency range is 0.01 Hz to 100 kHz. It is worth mentioning that the stimulus amplitude ranges from 10 mV - 2V. This instrument performs EIS analysis on cultural relics exposed to the outdoors, and the main component of relics is metal. Because the main components of the entire system are two Arduino development boards, the entire system is very light and portable. [38] Gerasta et al. developed a system based on AD5933 and a capacitive sensor, which is also controlled by Arduino (a microcontroller board). In the experiment, the capacitive sensor was placed in the metal solution. As the concentration of the solution decreases, the measured capacitance value increases at the same frequency[53].

For the biological applications Jaime Punter-Villagrasa et al. developed a complete set of a portable EIS device for hematocrit concentration blood analysis. The operating frequency of this device is between 10 Hz and 100 kHz. The signal-to-noise ratio (SNR) rejection reached -40 dB[54]. Ferreira designed a bio-impedance monitor system with a 4-electrode analog front-end (AFE) for wearable plethysmography applications. The working frequency is between 0-100 kHz, and the error is less than 1%[55]. The working frequency range of the design is 10 Hz -10 MHz. In the actual measurements, magnitude data can be obtained within the frequency range of 10 Hz - 3 MHz. Relatively accurate phase measurements can be obtained at 10 Hz – 20 kHz.

1.4 Design Goal and Challenge

The overall purpose of this work is to reduce the size and complexity of the impedance measurement system. The system should be able to perform an in-situ EIS analysis of the sample. We list several specific goals for us to design the system.

- The device is required to perform in-situ impedance measurement for the given sample.
- The magnitude accuracy should reach within 3% when measuring a pure resistor.
- The measurement should be comparable to the result of SP-200 in the frequency range of the EIS analysis of the corrosion sample.
- The impedance measurement data could be used as a source of the EIS analysis.

For this project, there are a lot of challenges to design the system.

- Firstly, the challenge is to decrease the testing signal's amplitude before the sample-under-test and amplify the response signal.
- Then the data acquisition system should collect the response signal data and send it to the PC for impedance calculation.
- Since sending the signal and receiving the signal are two different blocks, the synchronization between the two blocks should be guaranteed.

1.5 Thesis Outline

This thesis consists of five chapters to demonstrate an impedance measurement system dedicated to monitoring metal corrosion phenomenon. The thesis is organized as follows.

Chapter 1 gives an introduction to the metal corrosion phenomenon. Also, the basic idea of EIS analysis and its connection to metal corrosion is introduced. Two different EIS analysis equipment were shown. Besides, we reviewed some works that are similar or related to ours. The goals and challenges of the whole work are presented in Chapter 1.

In chapter 2, the purpose is to show the design of the impedance measurement system. We will introduce the hardware and the software of the system design of the system. For the hardware, the circuits in the system will be described one-by-one. The software design includes the data processing and impedance calculation methods.

The aim of chapter 3 is to test the performance of the impedance measurement system. Firstly, the accuracy of the system will be shown with experiments. Then, we use the system to perform a real EIS analysis on a corrosion cell. In the EIS analysis, the system was able to help the EIS analysis as an impedance measurement device. As a result, the system was able to reach the goals of the design.

Chapter 4 introduces the ongoing work on the impedance measurement system for the COVID-19 antibody test. And chapter 5 gives the conclusion of the whole thesis.

Chapter 2

Hardware and Software design of the Impedance Measurement System

In this chapter, we illustrate the software and hardware design of the impedance measurement system. Firstly, we dig into each of the circuit blocks of these systems. Then, we show the principle of measuring the impedance of our system. Finally, we conclude this chapter.

2.1 The system design of the impedance mea-

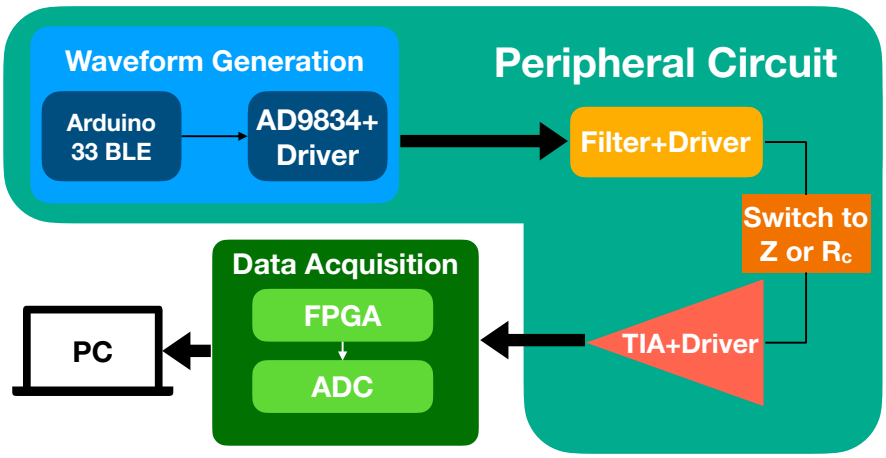

Figure 2.1: The block diagram of the Impedance Measurement System

The impedance measurement system was implemented using both the hardware and software. The hardware and the software of the system work together to accomplish the impedance measurement. Each of the modules has their own function. Some of the system blocks are commercially available product, and others are customized design for the corrosion impedance measurement. As shown in Figure 2.1, the design of our device consists of several modules. They are peripheral circuits, field-programmable gate array (FPGA)-controlled analog-digital converter (ADC) to convert the signal from analog to digital, and a personal computer (PC). The entire workflow is as follows.

- First, the Arduino sends control signals to AD9834 to generate a series of sine signals, which are applied to the peripheral circuit.
- The signals pass through the filters and drives, and then signals were applied to the load impedance (Z) or calibration resistor (R_C).
- The ADC then converts the voltage at the output of the trans-impedance amplifier (TIA) to a digital signal.
- The FPGA sends the signals to the PC for signal processing and impedance calculation.

After these steps, the impedance calculation result should appear on the screen of the personal computer. In addition to visualization, these data can also be stored as separate files and used to help EIS analysis. Next, we will dig into each of the blocks of the hardware design. Every block of the circuit will be introduced in detail. This will give us a better understanding of the principles and working methods of the entire system.

2.2 Hardware: Peripheral Circuit

In general, the purpose of the peripheral circuit in the impedance measurement system is as follows:

1. Generate a sine wave and level down the amplitude of the signal to make sure the proposed system is a potentiostat.

2. Filter out noises that could cause inaccuracy on the impedance measurement result.

3. Switching the signal between Z and R_C.

4. Transform the current signal that yields during testing to a voltage signal. And then, amplify the voltage signal to a proper amplitude for ADC sampling.

2.2.1 The Waveform Generation Circuit Design

An AD9834 20mW 75MHz DDS (Digital Direct Synthesis) controlled by an Arduino 33 BLE micro-controller functioned as the signal generator of the whole system. A series of sinusoidal signals were generated by AD9834. We use the AD9834 as the signal generator of the whole system. The signal from the AD9834 cannot be directly used on the sample-under-test because of the signal amplitude and the potential noise from the AD9834. The peak-to-peak value of the AD9834 output sine wave in the equation 2.1[56].

$$V_{peak-to-peak} = I_{fullscale} * R_{output-to-ground} = 3mA * 200\Omega = 600mV \quad (2.1)$$

The proper peak-to-peak value for our application should be around 50mV[8]. Such a 600mV is too big, and we need a driving circuit to level down the amplitude.

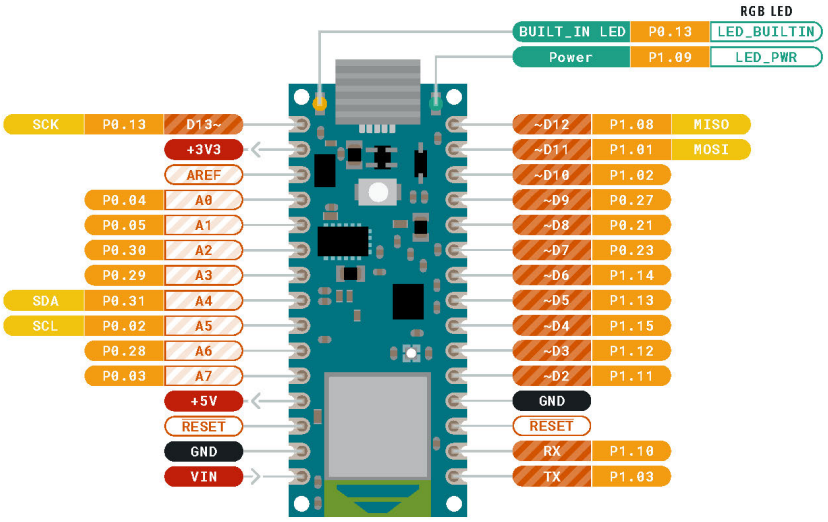

Figure 2.2: The Pinout Diagram of the ARDUINO NANO 33 BLE [57]

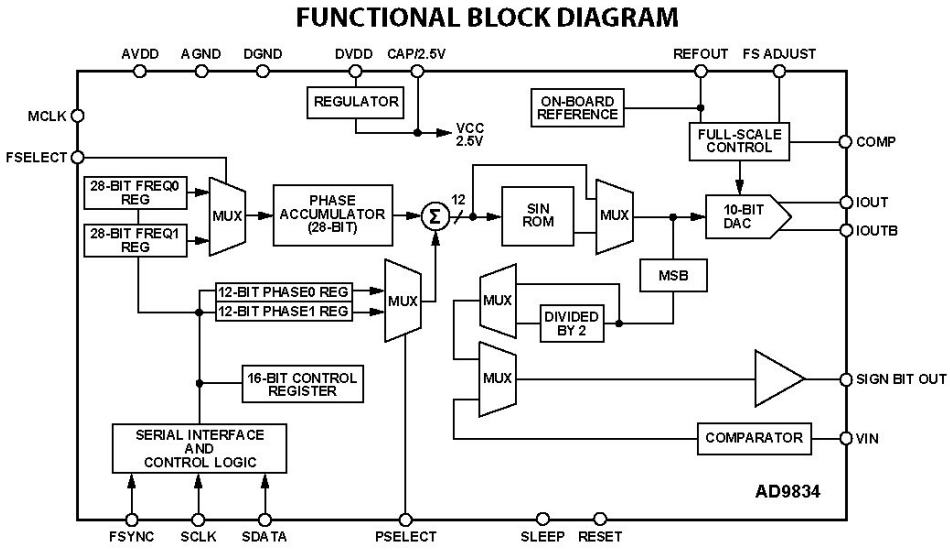

Figure 2.3: AD9834 Functional Block Diagram [56]

Figure 2.2 shows the pinout diagram of the Arduino Nano 33 BLE. Figure 2.3 shows the functional block diagram of the AD9834 DDS. When the signal is generated through the AD9834, the current signal comes out of the "IOUTB" pin. The "IOUTB" connects one end to the analog ground through a 200Ω

resistor and the next stage of the circuit. The voltage signal is detected since the current signal is loaded on the resistor.

For every different sine wave sent out by the "IBOUT" pin of the AD9834, there is always a corresponding control word loaded into the AD9834 "FSELECT" pin. The frequency and phase control worlds can determine the frequency and the phase of the sine wave. For our application, we need to control the frequency of the different sine waves. The phase for every different sine wave should remain the same. The reason is that we want to get the complex impedance value over a range of frequencies. There is no need to change of the phase of the testing signal.

There are four groups of signals in total as shown in Table 2.1, each corresponds to a specific ADC sampling frequency. The frequency range of the testing signal is from 10Hz all the way to 1MHz.Although some of the corrosion studies use sub-Hz waves to determine the corrosion reaction inside the corrosion cell, we used relatively larger frequencies because we want to achieve a quick measurement. The sub-Hz EIS is suitable for corrosion analysis. However, it will take a long time to conduct the experiment[58], [59]. For high-frequency signals, it takes less time to yield the same number of periods of signals than a low-frequency signal. We want to reduce the time for the experiment so that we increased the testing frequency. Also, a short testing time is suitable for an in-situ system.

The selection of sampling frequencies is based on the signal frequency. According to the Nyquist law, if the sampling frequency is lower than twice the signal frequency, aliasing occurs. Therefore, as a requirement of the measurement, there is a minimum value of the sampling frequency. Table 1 shows that from 10Hz to 200 kHz, the sampling frequency is at least 2.5 times higher than signal frequency. 100 MHz is the sampling frequency for the last group of testing signal, which ideally could handle frequencies up to 750 MHz. However,

due to the parasitic capacitance and inductance in the system, we could only obtain certain results under 1MHz. For the last group, we used a higher speed ADC than the other three groups. In the first three groups, we used a 12-bit ADC with a highest sampling rate of 500 ksps (kilo samples per second). The ADC used in the last group is 14-bit, and its highest sampling rate is 150 Msps (million samples per second). These two different ADCs are on the commercial board P0435 (Terasic Technologies, Hsinchu, Taiwan). In Table 1, the sampling frequency is converted through the sampling rate.

Table 2.1: The signal frequency and the corresponding ADC sampling frequency

Signal Frequency	10Hz-400Hz	500Hz-40kHz	50kHz-200kHz	300kHz-1MHz
Sampling Frequency	10kHz	100kHz	500kHz	100MHz

2.2.2 The Low Pass Filter Circuit Design

Before the signals are applied directly to the corrosion sample, a 6th-order Butterworth low-pass filter is used to minimize the high-frequency noise that may influence the measurement result. A low-pass filter is required before the signal is applied to the sample-under-test. The purpose is to minimize the influence of high-frequency noise[60].

Butterworth filter is a very commonly used filter. We selected the 6th order because the result is optimal for our application. The design of the entire filter is based on three operational amplifiers. Figure 2.4 shows the schematic of the filter. The "Vin" pin is the input signal source. The output of the operational amplifier(op-amp) is the output of the filter circuit. In figure 2.4 the "V2" source provides the bias of the circuit. Figure 2.5 shows the transfer function of the filter from 1-50MHz. The -3dB cutoff frequency is about at the 34MHz. This design is enough for the impedance measurement system to reduce the

impact of the high-frequency noise. We did not choose the Chebyshev filter, although it has a better frequency response. The reason is that we don't want to increase the complexity of circuit design more. Increasing complexity will increase the power consumption of the entire circuit and increase the difficulty of debugging.

We use a low-pass filter to eliminate high frequency noise[52]. For example, the frequency of the quantization noise from the digital-to-analog converter (DAC) in the AD9834 DDS is higher than the signal frequency. Filter circuit removes undesired noise, to obtain more accurate impedance measurement results. Driver circuits are also used before the input and after the output of the filter. The driving circuits are simply inverting op-amp circuits[61]. Generally speaking, for blocks with input and output signals, we intend to increase the input resistance and decrease the output resistance to isolate different stages of the system. In this way, the signal loss between each circuit stage could be less. Also, the driving circuit at the front of the low-pass filter leveled down the signal amplitude. Proper signal amplitude is required in EIS analysis on the metal corrosion phenomenon. The desired input signal is with around 50mV Vpp(peak-to-peak) amplitude[8]. Meanwhile, the driving circuit can guarantee that the signal output is relatively stable so that the proposed impedance measurement system can function as a potentiostat.

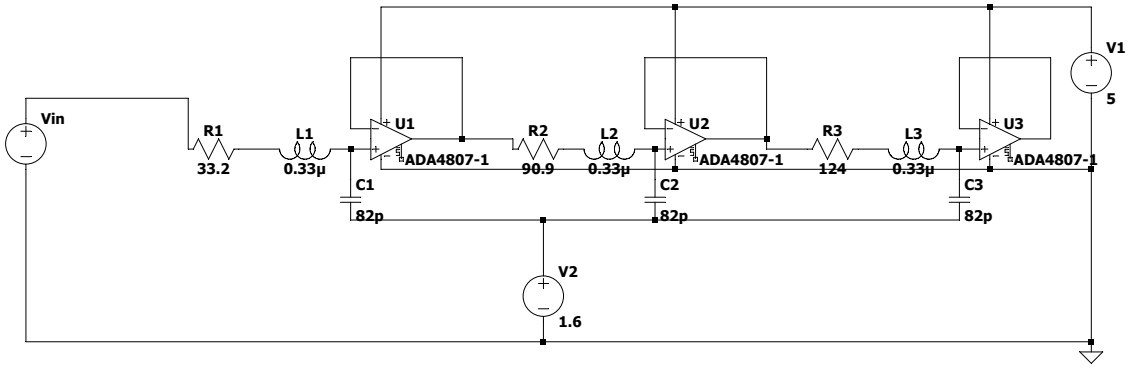

Figure 2.4: The low-pass filter schematic

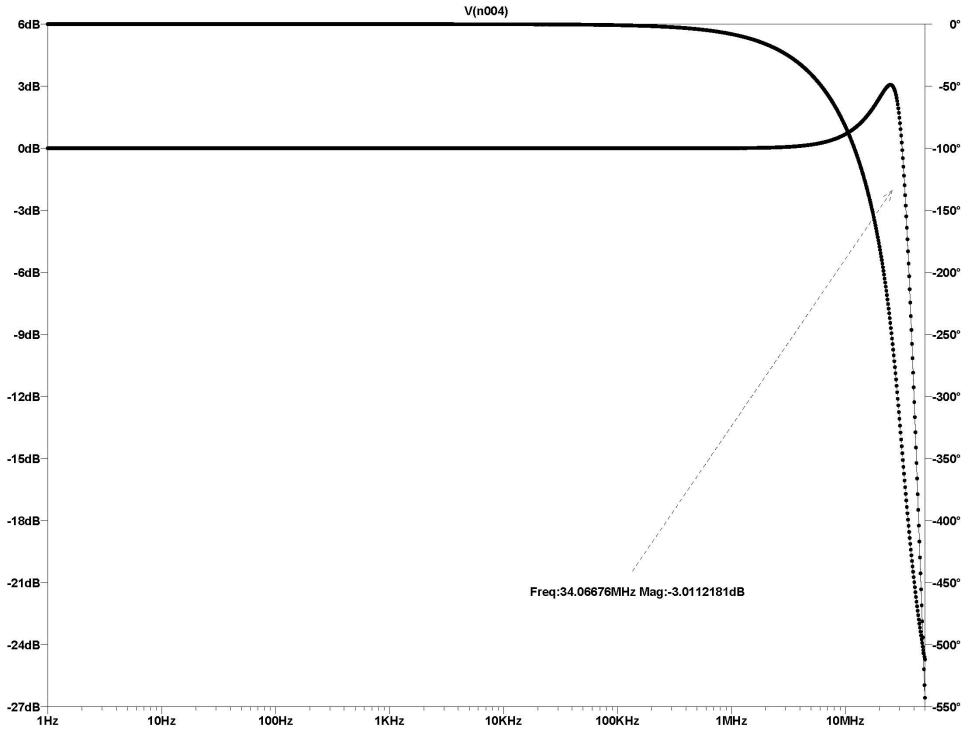

Figure 2.5: The low-pass filter transfer function

2.2.3 The Switching Circuit Design

An analog switch 74AUP2G57GUX (Nexperia BV, Nijmegen, Netherlands) controlled by the Arduino in the circuit can switch the signal between the calibration resistor and the corrosion sample. The analog switch is very situable

for the impedance measurement system due to its low-power consumption, wide supply voltage range, high-frequency and high-noise immunity.Figure 2.6 shows how we calculate the sample impedance (Z) using a calibration resistor (R_c) The first step is to connect the test sample to be tested and measure the current I_{x1}. The second step is to apply a voltage to the calibration resistor to get the current I_{x2}. Impedance can be obtained by equation 2.2. As mentioned above, the switching between Z and R_c is obtained using an analog switch.

$$Z = \frac{R_c \cdot I_{x2}}{I_{x1}} \tag{2.2}$$

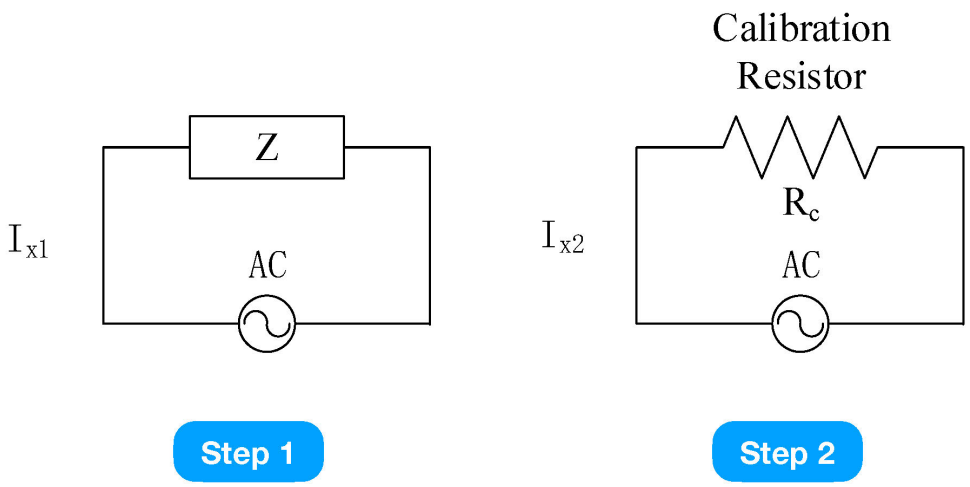

Figure 2.6: Steps used to measure the impedance.

2.2.4 The Transimpedance-Amplifier(TIA) Design

The output from the sample or calibration resistor is a current signal. However, a voltage signal is required for ADC to sample, and thus a trans-impedance amplifier (TIA) is required. Figure 2.7 is a schematic of the TIA. Since the signal to be amplified is very small(several tens of mV), four different stages of the TIA are used to achieve a high gain. The first stage converts the current to a voltage by feeding it to the R3 resistor. Because the sample's impedance

under test varies, the current feeds into the TIA are not constant. The output at the first stage is a sine wave of several tens of millivolts peak-to-peak. The following two stages are inverting an op-amp amplifier that can level up the signal. These two stages form a non-inverting voltage amplifier. Equation 2.3 gives the estimated gain of stage 2 and stage 3.In amplifier design, more stages can ensure a wider bandwidth while maintaining a certain gain. The purpose of C1, C3, and C5 is to keep the feedback loop of the op-amps stable.

$$A_u = (-\frac{R7}{R5}) * (-\frac{R11}{R9}) \approx 35 \tag{2.3}$$

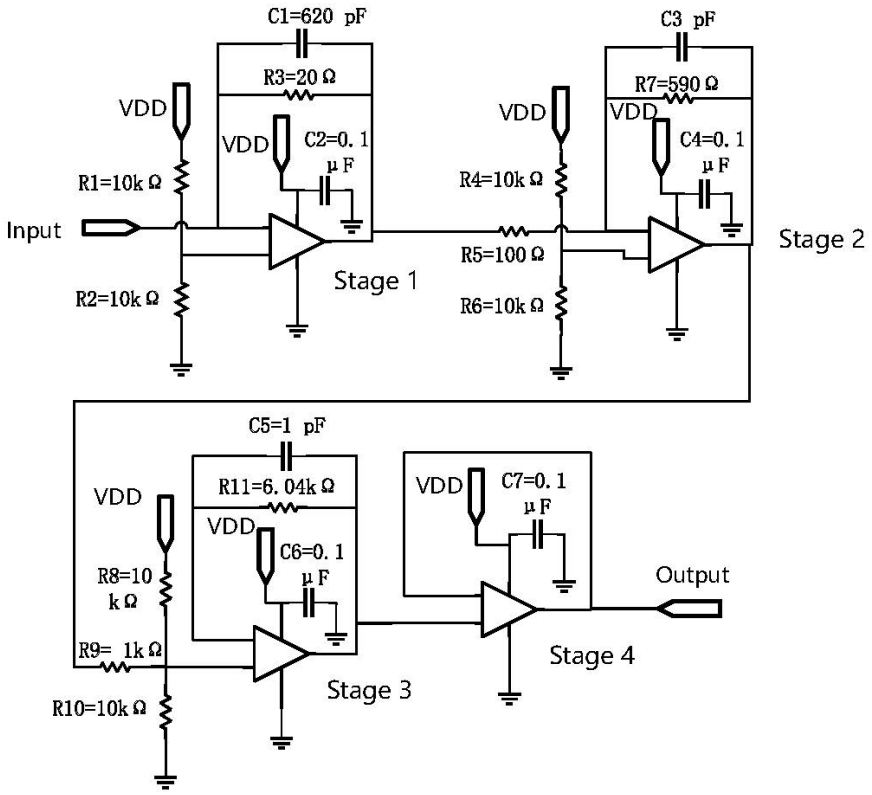

Figure 2.7: The TIA with driver used in the system.

The gain is about 35. Under this condition, amplifying a signal of several tens of millivolts could yield an output signal with a peak-to-peak value below 3.5V. The ADC input range is 0-4.096V, which is high enough for a signal with

a 3.5V peak-to-peak value so that the ADC can function properly. This is the reason why we choose the gain of 35. A voltage follower as a driver circuit is the stage 4 of the TIA.This stage serves as a driver.

Overall, the peripheral circuit's function is to generate a sine disturbance signal and feed it to a corrosion sample or a calibration resistor. Finally, by increasing the signal amplitude, the ADC can sample the signal more accurately.

2.2.5 ADC Sampling and Data Acquisition

Using the ADC, we converted the obtained analog signals into digital signals and processed the digital signals using a commercial board P0435 (Terasic Technologies, Hsinchu, Taiwan). On the P0435 board, there is an FPGA that can control the on-board ADC. We also select this board because of its portability and simlpicity of re-programming.The operating speed of this board is enough to perform the data acquisition. The signals were then sent to the PC for data processing. In this process, the synchronization between signal generation and data acquisition is crucial. Since the Arduino and FPGA are two different blocks, we set a 2-second time delay for each testing frequency in the Arduino code and FPGA code separately. At a specific time interval, the sine signal's output frequency from the AD9834 corresponds to the ADC sampling frequency. As a result, we can obtain the impedance result at a particular frequency.

Table 2.1 shows four different sampling frequencies that correspond to each group of sine testing signals. The ADC is controlled by a processor generated through Nios II App. The digital signal is transmitted to the PC and the data was saved into four different files according to the different sampling frequencies. After storing all the data into different txt files, we used them one by one for impedance calculation. For each separate file, the data was read

to a cell array first. We then calculated the frequency, magnitude, and phase of the signal. By performing fast Fourier transform (FFT) , we can obtain the magnitude and phase of the signal as shown in Equations 2.4 and 2.5. In Equation 2.4, I_{x2} [k] and I_{x1} [k] are the FFT magnitude result of the current through the calibration resistor and the sample under test, respectively. For the phase in Equation 2.5, θ_{x2} and θ_{x1} are the FFT phase result of the current through the calibration resistor and the sample under test respectively.

$$Amplitude = \frac{I_{x2}[k] * R_{CAL}}{I_{x1}[k]} \tag{2.4}$$

$$Phase = \theta_{x2} - \theta_{x1} \tag{2.5}$$

Figure 2.8 shows the implemented impedance measurement system. Some areas were colored with explanation, showing the position of different blocks.

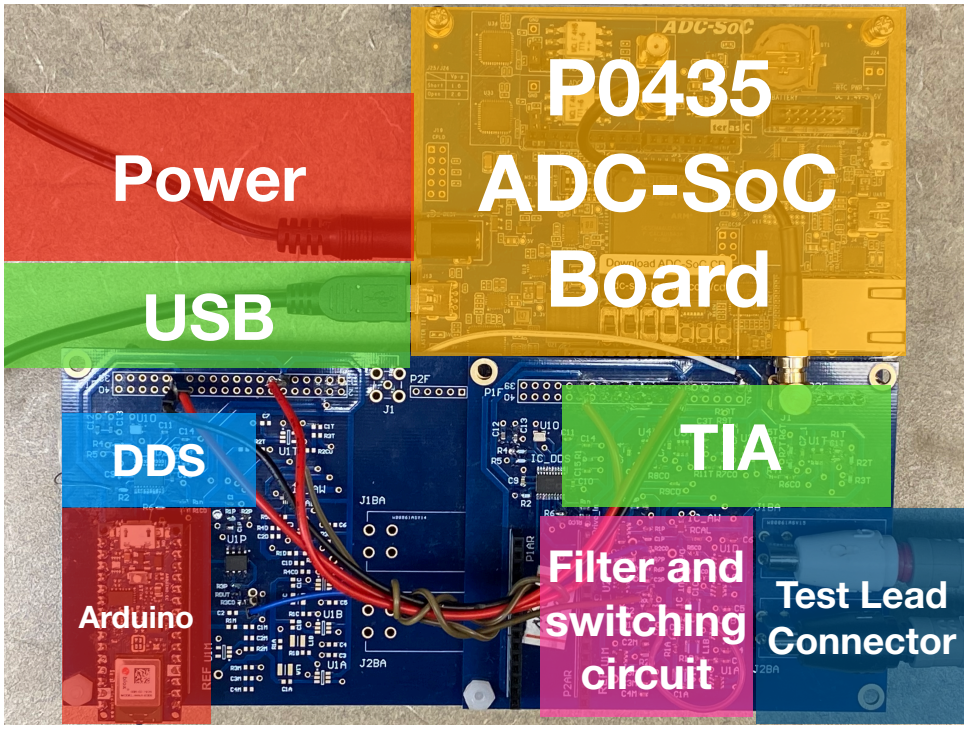

Figure 2.8: The proposed impedance measurement system

In addition to the circuit blocks introduced above, the figure also shows

some parts that have not been introduced. These parts are very important to our impedance measurement system. For example, the power supply interface also has a USB interface to ensure communication with the computer. There is also banana connector for test lead. The test lead is used to connect the impedance measurement system and the corrosion cell. Through the test lead, any sample-under-test is connected to the circuit and becomes a part of the circuit.

Regarding the software design of the entire system, this part is in data acquisition. Here we describe the working sequence of the software system. First, Graphical-User-Interface (GUI) was created. After that, the Nios processor will notify the ADC to prepare for sampling. Next is the impedance calculation part. All collected data will be stored in a txt file, and the file will be read into the cell array by the program. Through impedance calculation, we receive three return values, namely frequency, phase, and amplitude. These data are displayed on the graph.

2.3 Conclusion

In this chapter, we introduced the details of the impedance measurement system design. Every part of the hardware is described in detail. We showed the waveform generation circuit. The low-pass filter circuit was also described. In order to perform an impedance measurement, the switching circuit was used. Also, the data acquisition and the impedance calculation were illustrated. We have paid attention to a lot of details in the design to ensure that the entire system can complete the impedance measurement work.The system is ready for the performance evaluation and real test of the EIS analysis.

Chapter 3

System Evaluation and Corrosion Experiment Process

The method of instrument evaluation used in [52] for instrument evaluation can be used to analyze our experimental results. The entire instrument evaluation process in this paper is divided into two stages: the first stage is precision verification and the second stage is EIS analysis on a corrosion cell with metal sample.

1. In the first stage (precision verification), we used our instrument to measure resistors. The resistance is known in advance We then calculate the accuracy based on the measured values. Secondly, we measured a test sample consisting of two resistors and a capacitor. Finally, we compared the measurement results between the proposed impedance measurement system and the bench-top SP-200 EIS instrument.

2. In the second stage (EIS analysis), we measured the EIS impedance spectra of a corroded metal sample at different times, and then used the equivalent circuit for parameter fitting. The results of the fitting can explain the composition changes in the corrosion metal sample.

Besides the experiment, we will compare our system to the works that have been previously reported.

3.1 Precision Verification

This section contains two different parts. The first part shows the accuracy of the system. We test the impedance measurement with our system firstly on a pure resistor and then on a circuit model. Then we do the second part that demonstrates the impedance measurement system's ability to help EIS analysis.

3.1.1 Test on a pure resistor

For the precision verification, a series of resistors ranging from 10 Ω-150 Ω were used as the testing samples. These resistance values were selected because the impedance of the corrosion cell is within the range. The operating frequency used is 10 Hz-200 kHz. The resistor used in the experiment is the RS-201 resistance substituter (IET LABS INC. Long Island, New York, USA) with an accuracy of ±(0.1%+0.025 Ω). Since we are going to measure the magnitude and the phase of the resistors, we will calculate the magnitude and the phase error separately. Comparing with the Impedacne Measurement System results to the values of the pre-set resistance substituter, the measurement magnitude result error was calculated using equation (3.1) for each of the values of the resistors under a certain signal frequency. As a result, we can get a series of calculated errors for each resistor under a certain frequency. Taking the average of all the error data we collected, we can get the magnitude error=0.028.

$$error = \frac{|Z_{measurement} - Z|}{Z} \tag{3.1}$$

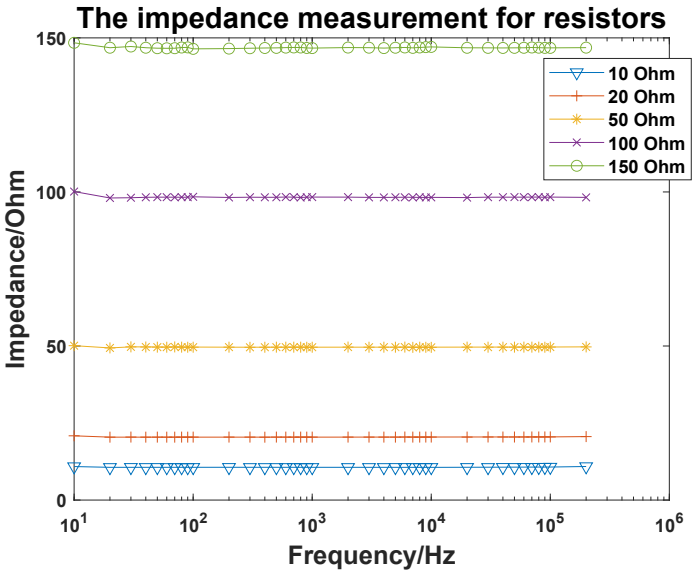

Figure 3.1: The measured impedance magnitude results of the resistors.

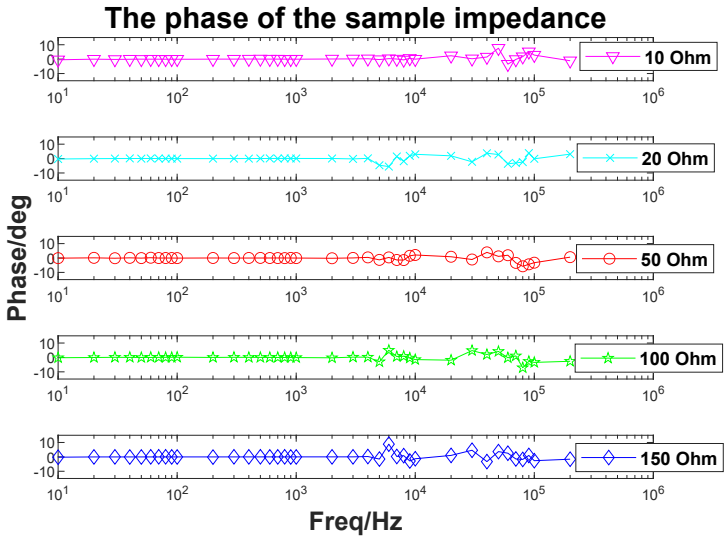

Figure 3.2: The measured impedance phase results of the resistors.

The ideal phase of the complex impedance of a pure resistor is 0, so we regard the absolute value of the phase result as the phase error. Table 3.1 shows the results of the error calculations. The phase error of the device is calculated by taking the average of all the calculated error results. In this case, for the proposed Impedacne Measurement System, the phase error is

1.051 degrees. Figure 3.1 shows the magnitude results of the resistors while the Figure 3.2 visualizes the phase result. As observed from the Figure, the measurement result remained relatively stable for each of the values of the resistors. The inaccuracy could come from the limitation of the device, such as the resolution of the DDS and ADC. Also, the parasitic capacitance in the whole system contributes to the inaccuracy in the final measurement result.

Table 3.1: The impedance magnitude and phase measurement error

Magnitude Result Error					
Frequency(Hz)\Resistance(Ω)	10	20	50	100	150
10	0.088	0.043	0.002	0.001	0.011
100	0.064	0.022	0.008	0.016	0.024
1000	0.063	0.022	0.008	0.017	0.022
10k	0.063	0.022	0.008	0.018	0.020
100k	0.072	0.025	0.007	0.017	0.021
200k	0.089	0.030	0.006	0.018	0.021
Phase Result Error					
Frequency(Hz)\Resistance(Ω)	10	20	50	100	150
10	0.448	0.297	0.102	0.200	0.233
100	0.020	0.017	0.064	0.160	0.076
1000	0.367	0.069	0.060	0.105	0.047
10k	0.001	2.980	2.101	1.496	1.311
100k	2.813	0.139	3.256	3.447	2.657
200k	1.104	3.073	0.590	2.669	1.621

The next step is to compare the proposed Impedacne Measurement System and a bench-top commercial instrument, the SP-200 Potentiostat (Biologic, France). This impedance meter is a single-channel transportable potentiostat workstation. To compare the results, a sample is required. Figure 3.3 shows the circuit model that was used as the sample for testing. The circuit model can represent the electrochemical behavior of a homogenous metal solution interface [39].

The selection of parameters is based on the equivalent circuit parameter fitting result from the EIS spectra of a corrosion cell.

Figure 3.4 and figure 3.5 show the comparison of the measurement magni-

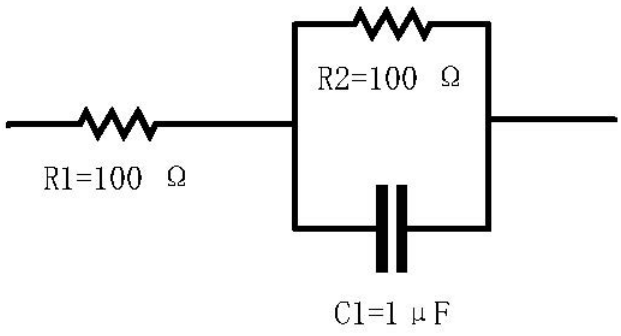

Figure 3.3: The circuit model as sample under test.

tudes and phases, where the starting frequency is 10 Hz, and the stop frequency is 6kHz.

The results of the proposed Impedacne Measurement System showed the same trends as the commercial SP-200. Our results are slightly lower than those of the SP-200 within the whole testing frequency range. The inaccuracy of the measurement result is likely due to the limited accuracy of the AD9834 DDS. At low frequencies, the result deviates from that of the SP-200. Replacing the crystal oscillator (75 MHz) to a smaller value would improve the result. However, in that case, the frequency range would be shorter after replacing the crystal oscillator. The magnitude of the sample decreases over frequencies. This is because the circuit contains a capacitor and two resistors. Equation (3.2) shows the impedance of the circuit in Figure 3.3. R2 is connected in parallel with C1, and the whole is connected in series with R1. ω is the angular frequency of the signal passing through it.

$$Z(\omega) = R_1 + \frac{R_2}{1 + j\omega R_2 C_1} \tag{3.2}$$

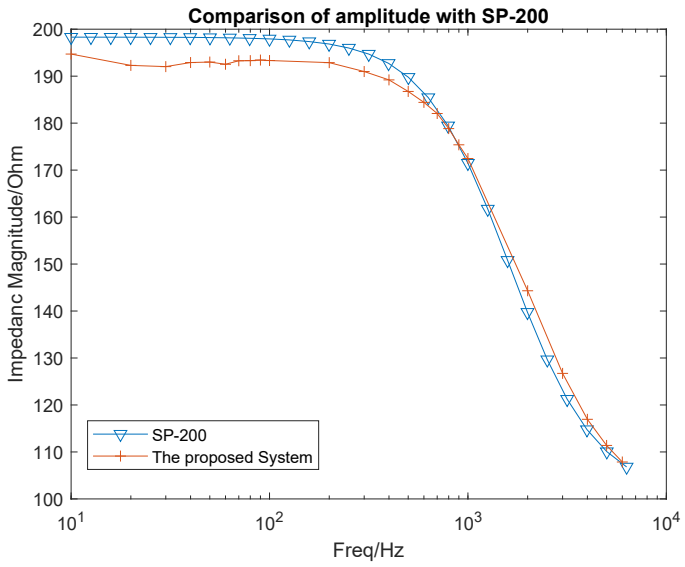

Figure 3.4: Compare the magnitude result to SP-200

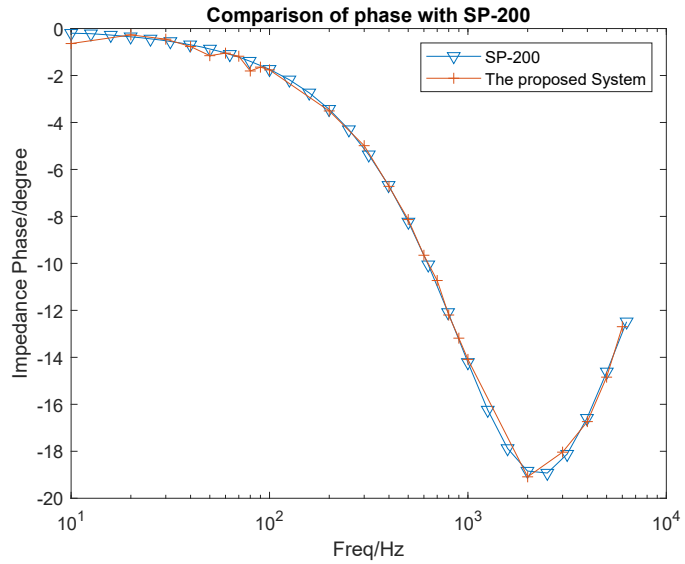

Figure 3.5: Compare the phase result to SP-200

Because of only one capacitor in Figure 3.3, there is only one time constant in the circuit. As the frequency increases, the magnitude gradually drops. At low frequencies, the results about equal to R_1+R_2. At 6 kHz, the results approximately equal to the value of R1. Up to 6 kHz, the performance of Impedacne Measurement System is good. For the phase results, the two sys-

tems matched perfectly. In all, Impedacne Measurement System showed good compatibility and accuracy, and thus we can use it for the EIS analysis for the corrosion study.

3.1.2 EIS Analysis with a Corroded Metal Sample

Corrosion cells are often used to perform EIS analysis [8]. Consequently, a simple and portable corrosion cell was prepared for the in situ experiments [40], [62]. Figure 3.6 shows the corrosion cell that we used in our experiments. The corrosion cell (model CM2) was manufactured by Fourien Inc. (Edmonton, AB, Canada). During a corrosion experiment, a metal sample is fixed vertically on the corrosion cell. One end is exposed to the air, and the other end is exposed to the solution. The purpose of positioning the metal sample in such a way is to build a direct connection between the corrosion cell and the measurement system to minimizing any errors. There are inlet and outlet tubes connecting the two ends of the corrosion cell. By circulating the electrolyte solution (3.5% NaCl, about 2ml/s speed) in the corrosion cell rather than rotating the metal sample in the solution as a conventional corrosion cell, we get rid of a bulky motor and reduce the cost of the metal corrosion monitoring setup. 3.5% NaCl solution is commonly used in the metal corrosion experiment; for our experiment, we adopt this 3.5% NaCl solution [8]. During experiments, a peristaltic pump drives the solution to flow cyclically from the inlet to the outlet. For different experiments, we can easily replace metal samples. Table 3.2 shows the composition of the metal sample that we use for the corrosion. The sample is categorized as low-carbon steel(LCS).

Table 3.2: The composition of the low carbon steel sample

Material	Composition
Carbon	0.13-0.20%
Manganese	0.30-0.90%
Phosphorus	0.04% Max
Silicon	0.15-0.30% Max
Sulfur	0.50% Max
Iron	Balance

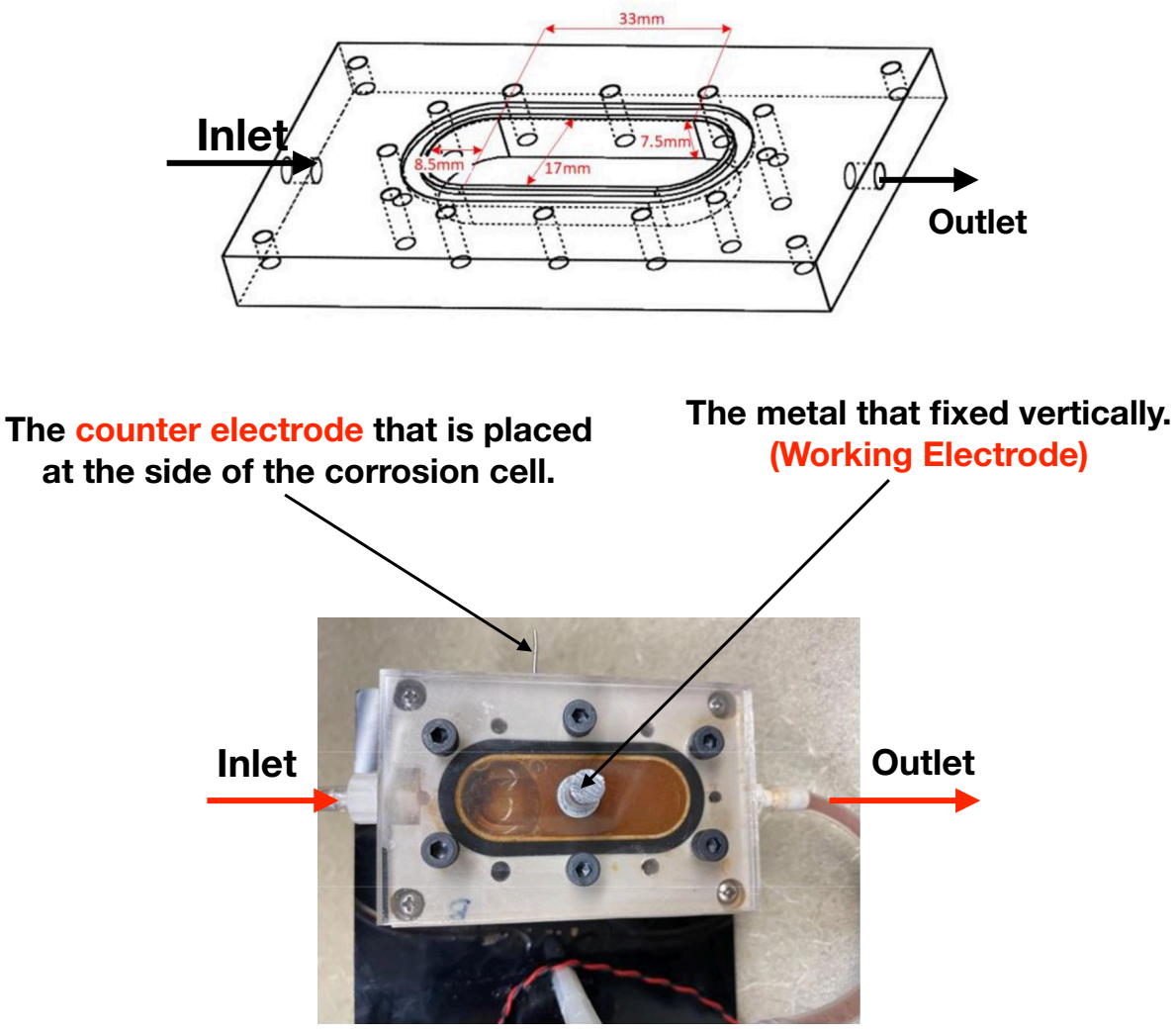

Figure 3.6: A 3-D diagram showing the dimensions of a corrosion cell. (Up) A real corrosion cell. (Down)

In the experiment, the peristaltic pump's 3.5% NaCl solution was driven to flow through the metal sample in the cavity evenly. We tested the impedance of the sample every two hours and recorded the results. At the beginning of the experiment, the liquid in the cavity was clear and transparent. However, after 10 hours, some precipitations began to appear in the cavity because the iron in the metal sample was oxidized and became rust. Figure 3.6 (right) shows the color of the liquid in the cavity when precipitation occurred. In a 72-hour experiment from [8] of a single-layer coating system in the 3.5% NaCl solution environment, the impedance changed significantly in the first 4 hours. In the following hours, the impedance also changed at a relatively steady rate. For our experiment, a time period of 10 hours is enough to observe our sample's corrosion phenomenon. Also, in [8], at the beginning of the experiment, a time interval of 2 hours was taken for monitoring, which is feasible for us in our experiment. During the experiment, we collected a total of 6 groups of data, and the corresponding time is 10 hours. The frequency range during each data collection is 10 Hz – 5 kHz. In EIS analysis for metal corrosion, the lowest frequency is essential due to the diffusion phenomenon that can be detected [20]. In our experiment, the selection of the lowest signal frequency is 10 Hz, which is a trade-off between the EIS analysis requirement and the testing efficiency. The selection of the highest frequency of 5 kHz is based on the result of the precision verification. In the precision verification that was presented earlier, the highest frequency was 6 kHz. The selection of 5 kHz can make sure that the proposed Impedacne Measurement System works in a typical frequency region. All the impedance magnitudes were shown in Figure 3.7, we can see that the impedance magnitude decreases as testing time elapses (2 hours, 4 hours, etc.). This confirms that most corroded surfaces are capacitive in nature. From Figure 3.9, we can see that at the same measurement frequency (10 Hz, 100 Hz, 1 kHz, and 5 kHz), the impedance magnitude de-

creases as time prolongs. There are two reasons that can explain the decrease in impedance. The first reason is that the surface of the metal was corroded, and the protective function of the surface gradually decreased.

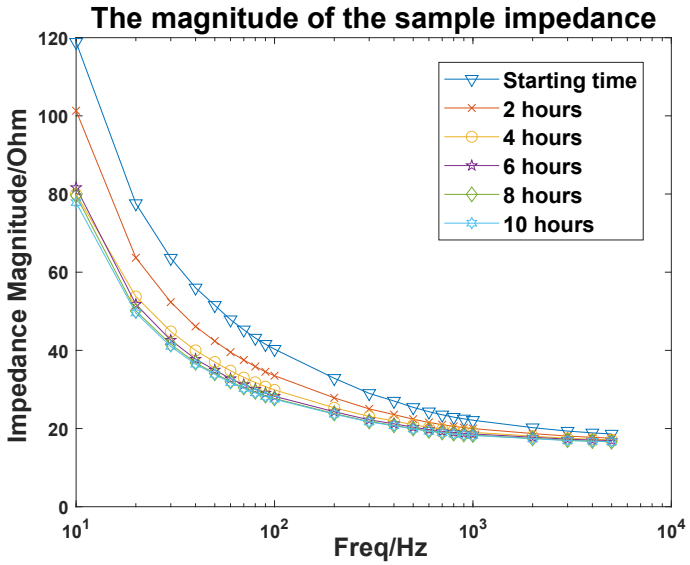

Figure 3.7: The magnitude of the impedance of the sample.

Another reason is that the resistance of the solution decreased because of the increased impurities in the circulating solution [8]. Based on the result of the precision verification, we choose to do the EIS experiment in the frequency range of 10 Hz to 5 kHz to obtain the best result. The detail of this behavior is explained further in the following experiment.

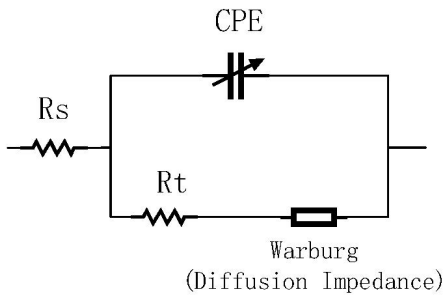

Figure 3.8: The equivalent circuit

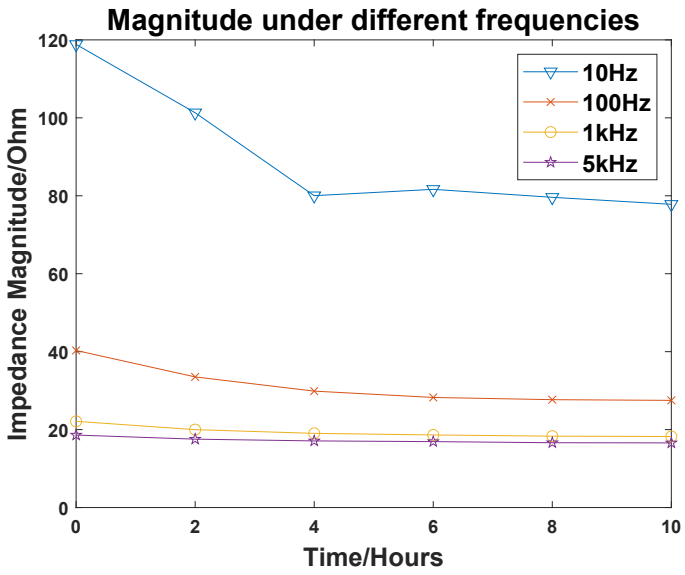

Figure 3.9: The comparison of magnitude under different frequencies

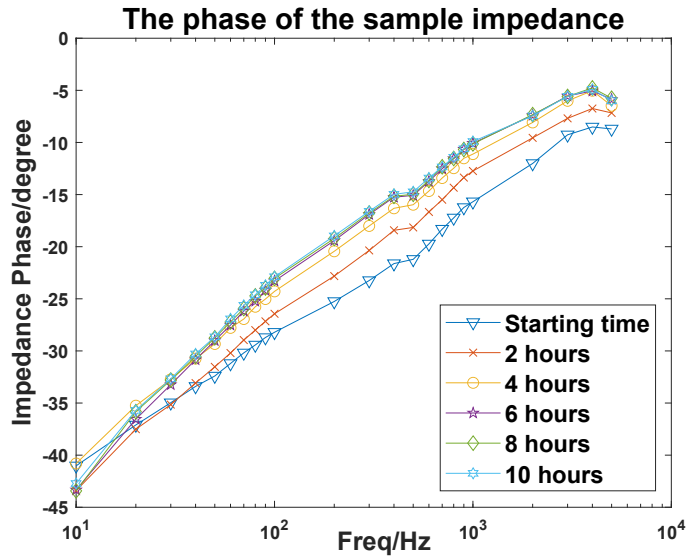

Figure 3.10: The phase of impedance of the sample

Figure 3.10 shows the measured phase of the impedance of the sample. As frequency increases, the value was closer to zero degree. With the magnitude and phase data, we can use an EIS equivalent circuit (Figure 3.8) and data fitting to understand what happened to the corrosion cell over time. According to the characteristics of our model, we selected an equivalent circuit model as

Table 3.3: The fitting result of EIS data

Time	Rs Ω	CPE: Q F*s^(α -1)	CPE α	Rt Ω	Warburg constant: Ω * s^(-0.5)
0 hour	16.92	0.202e-3	0.7161	20.40	681.8
2 hours	16.04	0.537e-3	0.6406	20.01	876.9
4 hours	15.95	0.522e-3	0.6665	15.23	590.4
6 hours	15.93	0.856e-3	0.6297	17.45	920.2
8 hours	15.67	0.870e-3	0.6301	16.71	857.0
10 hours	15.59	0.867e-3	0.6297	15.29	806.7

shown in Figure 3.8 [63]–[65]. The selection of Randles cell is based on the corrosion cell's capacitive nature and the fact that the corrosion reaction here is mainly controlled by the mass (oxygen) transport stage that happens on the surface of the metal sample [63].

For the EIS fitting software, we used EC-LAB (BioLogic Science Instruments, Seyssinet-Pariset, Auvergne Rhone Alpes) software to fit the data. The fitting methods were "Randomize and Simplex ". In this method, the software randomly selected parameters for fitting. The software searched for optimal initial values. The next step was simplex minimization, which was often used to minimize linear functions. Through the optimization of these two steps, we could obtain relatively accurate equivalent circuit parameters [60]. The fitting of each set of data has a total of 5000 iterations. Table 3.3 shows the result of the data fitting, where we have listed the parameters of the equivalent circuit at the different time points of measurements.

In the circuit, Rs represents the resistance of the electrolyte solution [39]. The value of Rs is closely related to the factors such as the concentration of the solution and temperature. As the corrosion reaction progresses, the composition of the electrolyte solution in the corrosion cell evolves over time, and the conductivity of the solution changes; as shown in the Table 3.3, Rs will also vary as the reaction progresses. For the constant phase element (CPE), its impedance is given in the Equation (3.3). In the equation, Q is

the CPE value. CPE is an element that can model the behavior between a pure capacitor and a pure resistor. α is the exponential value that determines the CPE model's characteristic and takes the value between 0 and 1. When α=0, the CPE model is purely resistive. On the contrary, when α=1, it is strictly capacitive. The constant phase element is related to the double-layer capacitance that represents the capacitance of the electrical double-layer that sticks to the metal sample surface. CPE is used instead of an ideal capacitor model because we want to obtain a more accurate fitting result [66]. The value of α for which the value usually lies between 0.5 and 1 shown in the table is related to the surface roughness [66]. During the experiment, the exponential behaved in a trend of decreasing over time, indicating that the surface roughness increased during the experiment [67].

$$Z = \frac{1}{Q(j\omega)^{\alpha}} \tag{3.3}$$

The charge transfer resistance shows the difficulty of the charge to transfer between substances during the corrosion reaction on the surface of the metal. As shown in the Table 3.3, the value of Rt dropped as time prolong in the experiment. The study finds that the decrease is related to the chloride ion facilitate the corrosion on the carbon steel. $FeCl_2 \cdot 4\,H_2O$ as a mid product for the reaction that accelerates the reaction of the iron [68]. The mass transport stage controls the corrosion reaction of the steel as one of the mass transport stage mechanisms. The diffusion of oxygen plays an essential role in the reaction. In the equivalent circuit, as shown in 3.8, a Warburg impedance element is used.

$$Z_W = \sigma(\omega)^{-0.5}(1 - j) \tag{3.4}$$

Equation (3.4) shows the impedance of the Warburg element. It is no-

Table 3.4: Comparison the proposed Impedacne Measurement System to other devices

Device	SP-200 Workstation	Arduino-based EIS system[38]	Impedance Detection Circuit[51]	This work
Accuracy	±0.03%	<5% for Magnitude. <3° for phase	±3%	±2.8%magnitude,1.051°error in phase
Effective Frequency Range	10 µHz to 7 MHz	0.01 Hz-100 kHz	up to 100 kHz	10 Hz-200 kHz(Resistor), 10 Hz-5 kHz(EIS)
Is it potentiostat?	Yes	Yes	No	Yes
Application	Multiple	Metal Corrosion Monitoring	Bio-molecules Detection	Metal Corrosion Monitoring

ticeable that the absolute value of the real part and the imagined part of the Warburg element are the same. In the Equation (3.4), σ is the Warburg constant. The value is related to the angular frequency and the constant. When it comes to the corrosion reaction here, the Warburg constant reflects the diffusion ability of the oxygen. The value of the Warburg constant didn't change rapidly with the accumulating rust layer. The behavior is interpreted as the oxygen does not need to permeate the rust layer to participate in the reaction [63].

Table 3.4 shows the comparison of the proposed Impedacne Measurement System to the other 3 different devices. The commercial SP-200 workstation listed in the table is a benchtop machine with outstanding performance. Compared to the other two works in reported literature, the proposed Impedacne Measurement System shows the good capability to conduct EIS analysis on the metal corrosion sample.

3.2 Conclusion

In this chapter, we performed a series of tests on the proposed impedance measurement system. The tests showed the system's accuracy when the performed impedance measurement. In the precision verification stage, we measured the impedance of a pure resistor and a circuit model. The system showed good performance and the potential of conducting EIS analysis. After that, we performed the EIS analysis on the corrosion cell. The system showed the ability to conduct an EIS analysis so that the design goals are achieved.

Chapter 4

Introdution to ongoing work: Impedance-Based COVID-19 Antibody Detection System

COVID-19 (Coronavirus disease) is a global health crisis that started at the end of 2019[69], [70]. Other than threatening lives and the public health system, the impact of this pandemic is long-lasting and overwhelming in many different aspects of human life, such as mental health[71]–[73] and economics[74]–[76]. According to data from Johns Hopkins University, as of May 31, 2021, there have been 170 million positive cases, and more than 3 million people have died of COVID-19 worldwide[77]. In Alberta, as of the end of May 2021, there were more than 220 thousand identified positive cases, and more than 2,000 people died as a result of the COVID-19[78].

COVID-19 patients are infected with 2019-nCoV and develop symptoms such as fever, cough, and shortness of breath[79]–[81]. In addition to the above symptoms, low-grade fever and mild fatigue are very common symptoms for patients with mild illness[82]–[84]. But for patients with more serious illness, infection can lead to pneumonia, severe acute respiratory syndrome, organ failure, and even death[85], [86].

In order to fight against this virus, the first thing to do when facing a patient is to detect whether the patient carries the virus or antibody in their body[87], [88]. In order to detect the virus, nucleic acid testing can effectively detect whether the patient is currently infected by the virus[89]–[91]. The

genetic material of this virus is RNA[92], [93]. If we detect the corresponding genetic material in the patient's body, then we can determine whether the patient has been infected[94].

In addition to nucleic acid testing, we can also perform antibody testing for COVID-19[95]. Antibodies are proteins produced by the human immune system after a person is infected with a virus or vaccinated[96]. The purpose of antibody testing is to determine whether the patient has ever been infected with COVID-19[94].

EIS analysis has been used in many different areas. The reason for this is that EIS analysis is very convenient. And EIS analysis can give us a lot of information about the tested sample. From this information, we can learn about the different reactions of the tested sample. As mentioned in the previous chapter, EIS can be used to detect metal corrosion. In this chapter, the main application of EIS analysis we discussed is in virus antibody detection.

The purpose of this chapter is to give a brief introduction to the ongoing work of the impedance measurement system dedicated to the COVID-19 antibody test in our research group. Compared to the original impedance measurement system for corrosion monitoring, the new system has some improvements that target a more efficient impedance test that helps EIS analysis on the given sample.

The organization of this chapter is as follows: Firstly, we do a brief literature review that can give some background information on why we need an impedance measurement system for the COVID-19 antibody test. After that, the COVID-19 impedance measurement system is based on the corrosion one; we will introduce the system's design and highlight what the improvement is compared to the previous one. Because the author is responsible for the analog front end (AFE) design of the system, the improvement of the AFE will be explicitly addressed. The testing result for the system is given as well to show the performance of the device. Finally, the conclusion summarises this chapter.

4.1 COVID-19 antibody lab-on-chip test with electrochemical biosensors

Lab-on-chip technologies have been used for COVID-19 tests. Currently, there are several commercial products available for rapid COVID-19 tests that are on the market[97].

Sahar et al. reviewed the electrochemical biosensors that are designed for the rapid diagnostics of SARS-CoV-2. The basic principle of the electrochemical test relies on the binding between the target substance in the sample and the immobilized substance on the surface of the electrode[98]. In other words, the fact that virus antibodies or antigens exist is ultimately transformed into a change in impedance. We can further infer whether there are antibodies or antigens by measuring changes in impedance.

Jesus et al. developed a handheld point-of-care system to perform a nuclear acid test for the SARS-CoV-2 within 20 minutes. The test sample passes through the microfluidic device, and this step performs the amplification of the viral genetic material. Finally, the tests are carried out. In a population of 183 with 127 positive samples, this instrument showed 91% sensitivity and 100% specificity. This system is more than just a nucleic acid detection device. This system can link nucleic acid test results with geographic information to form epidemiological surveillance of infected persons[99]. Although this system does not have an impedance detection device, it provides us with a new direction for virus detection. That is to test samples, collect data, and finally perform large-scale data analysis.

Rashed et al. successfully conducted SARS-CoV-2 antibodies rapid detection with impedance-based detector through EIS analysis. The SARS-CoV-2 antibodies at clinically relevant concentrations were used as samples on the sensing electrodes in their study. The study shows the feasibility of using EIS analysis to detect the SARS-CoV-2 antibodies with a commercially available impedance analyzer [100].

Among these detection methods, impedance detection devices play a very important role. The focus of our work here is to design a circuit system that

can effectively help with detection.

4.2 The system design of the COVID-19 antibody impedance measurement device

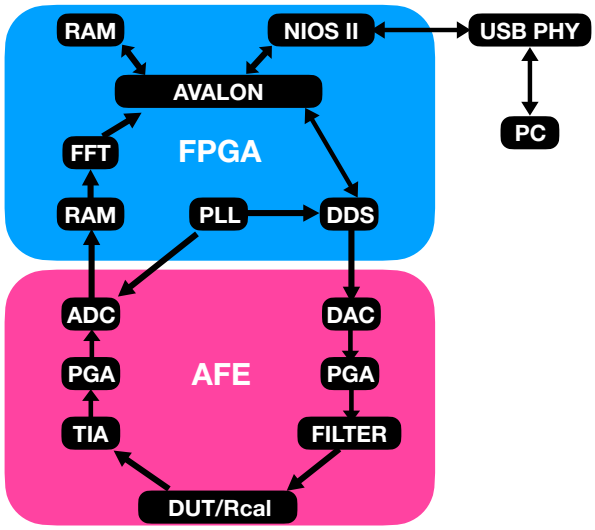

Figure 4.1: The block diagram of the impedance system of the COVID-19 project

Compared with the system used for corrosion detection, this system has many improvements. The main improvement is not only in the analog-front-end (AFE), but also in the overall architecture. Fig 4.1 shows the new block diagram of the new impedance measurement system. The corrosion one involves Arduino and FPGA as the control units for different circuity blocks that work separately. The original idea is to make a fast prototype of the whole system by eliminating the design complexity on each side. This is time, in order to seek a compact design, we only selected FPGA as the control unit.

In this section, we first introduce the analog-front-end(AFE) design and then present the FPGA design as the control unit.

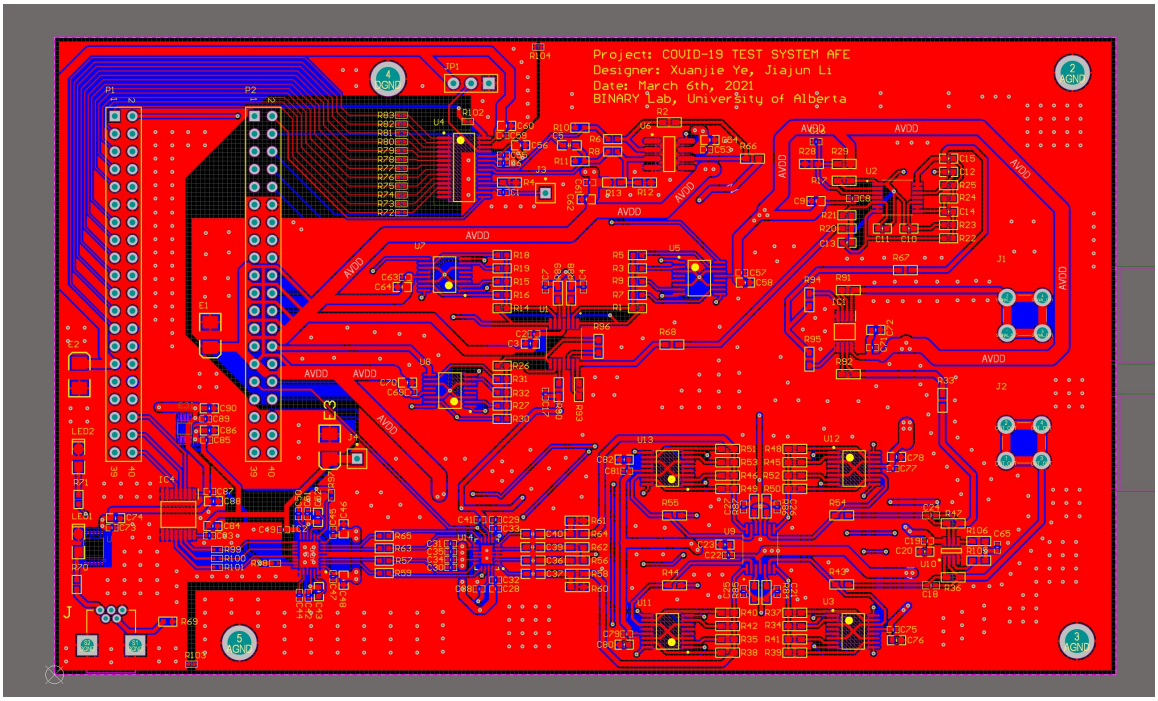

Figure 4.2: The PCB design of the impedance board for COVID-19 project

Figure 4.2 shows the PCB design of the impedance board for the COVID-19 project. As said in the previous chapters, the target impedance and the working frequency range for any impedance measurement system are very important parameters. Since the impedance measurement system for the COVID-19 system is supposed to work with the point-of-care system developed by other members in our research group, the target impedance range and the frequency range are set by them. The target impedance range of the new board is around 10^3-10^5 Ohm. The required frequency could be as low as 10 Hz and as high as 10^5 Hz.

For the target impedance range, the main job is to set a proper amplitude of signal across the sample under test. For the working frequency range, we should select the devices with a high gain-bandwidth product and adjust the gain on each level of the amplifier circuit.

4.2.1 AFE-Digital-Analog Converter(DAC)

In the corrosion one, we used an AD9834 DDS chip that has a DAC block inside the chip already. This time, the DAC is an independent chip AD9742

(Analog Device Inc.).

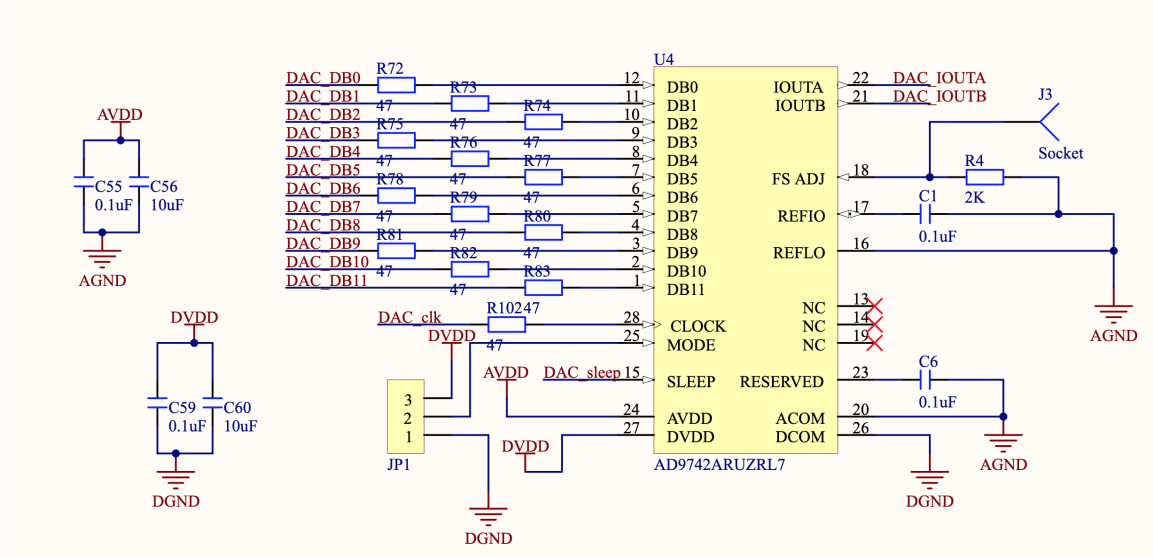

Figure 4.3: The DAC and the pin connection.

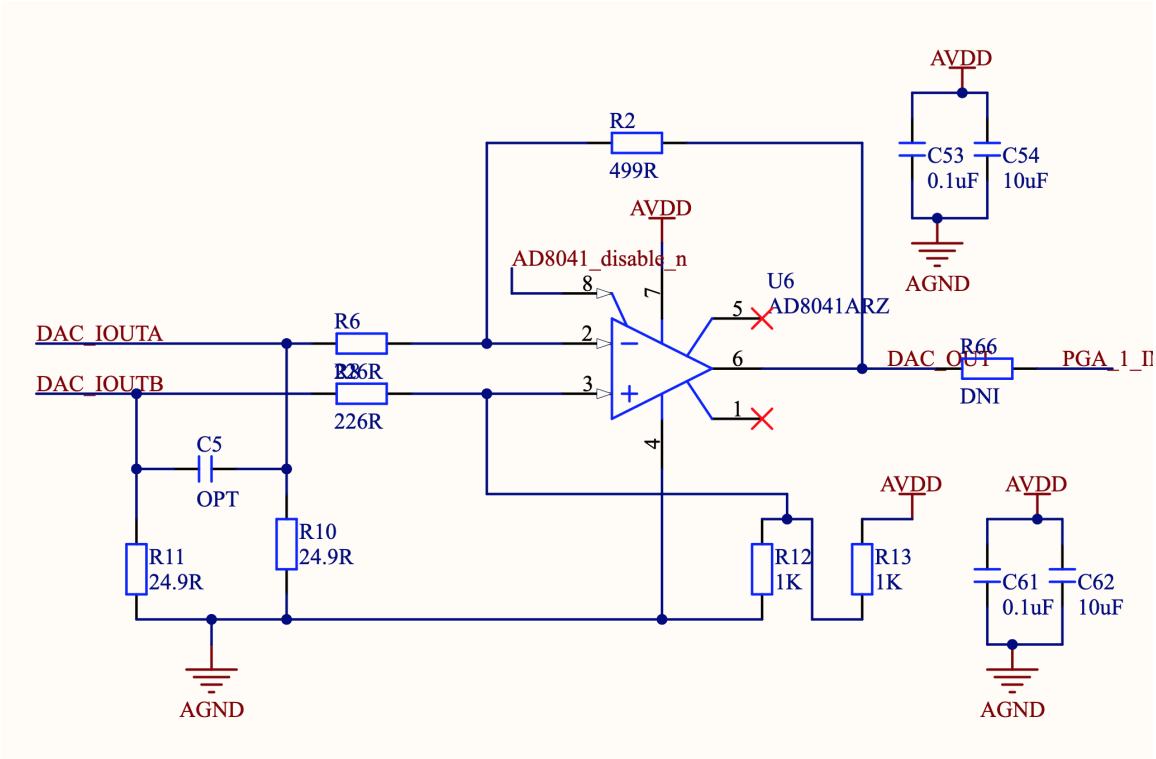

Figure 4.4: The DAC driver circuit.

Figure 4.3 shows the DAC chip and the pin connection of the AD9742. DB0-DB11 corresponds to the general-purpose input and output(GPIO) to

the FPGA development board. We can control the signal frequency from these ports. DCA-clk is the clock signal from the PLL on the FPGA board. We left a test point for the "MODE" pin to test the input data format. It could be either be binary or 2's complement [101].

The "IOUTA" and "IOUTB" are the output of the DAC chip. The signals from the two output pins are differential. We select a DAC driver as shown in Figure 4.4. The purpose of this driver is to make a differential-to-single-ended conversion of the output signal[101].As a result, the signal amplitude can be around 1V at the output of the DAC driver.

4.2.2 The programmable gain amplifier (PGA)

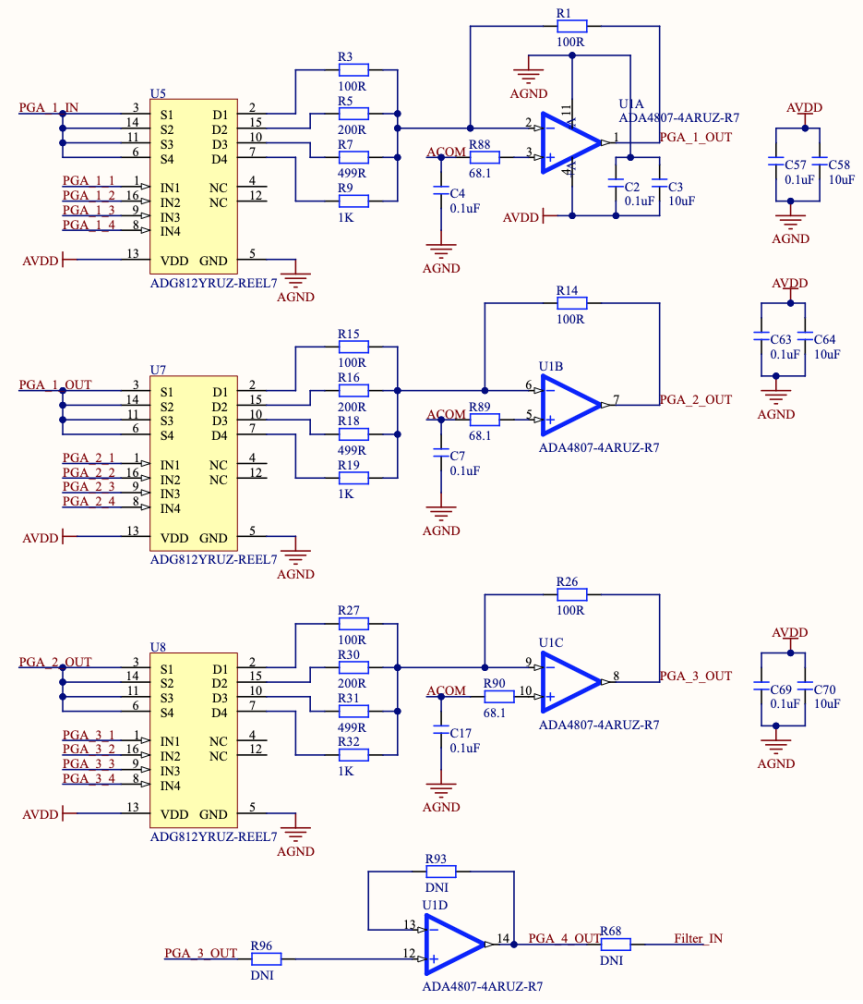

Figure 4.5: The programmable gain amplifier (PGA) circuit.

For the COVID-19 project samely, to perform an EIS analysis, we need to make sure that the signal applied across the device-under-test(DUT) or the calibration resistor is small enough because we need to make sure that the test is linear, causal, and stable[20]. Compared to corrosion one, in which the input amplitude is fixed, the new one can change the amplitude of the testing signal. We can change the testing frequency and the signal amplitude as well for the COVID-19 impedance testing sample.

Figure 4.5 shows the schematic of the PGA. The idea of the PGA is pretty straightforward. It is clear that we cascaded three simple op-amp feedback circuits together. It is noticeable that we used several ADG812 analog switches in the circuit. These analog switches aim to switch the resistors in the circuit to change the gain on each stage. For each of stage, the gain could be 1, 0.5, 0.2, or 0.1. Also, from the schematic, there is a voltage follower at the end of the PGA. The purpose is to make sure that the isolation between different stages.

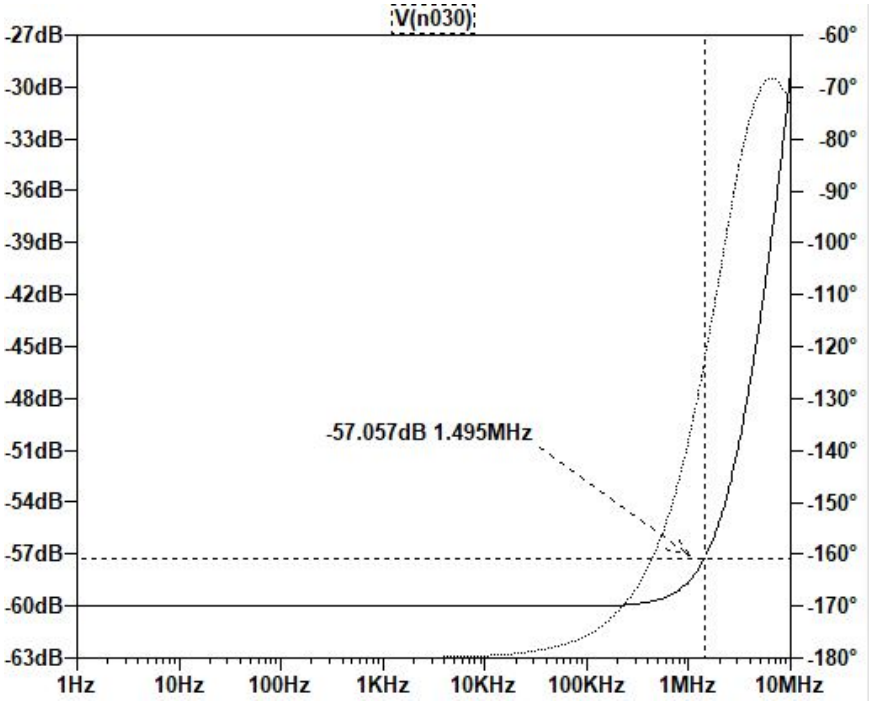

Figure 4.6: The AC response of the PGA

Figure 4.6 shows the ac response of the PGA when the gain=0.001(-60dB),

which means that the gain on each stage is 0.1(-20dB). From the simulation result, the bandwidth reached 1.495MHz. We have to pay attention to the bandwidth limit of each stage of the circuit because we want to have a relatively high-frequency testing signal so that we should be able to collect more information about the sample.

4.2.3 The low-pass-filter (LPF)

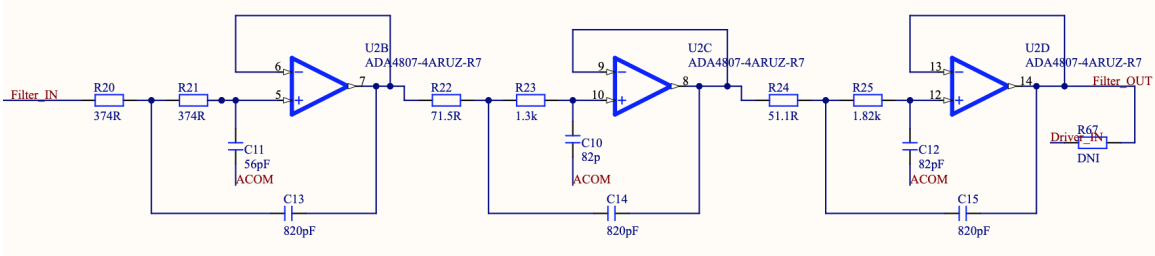

Figure 4.7: The schematic of the Filter

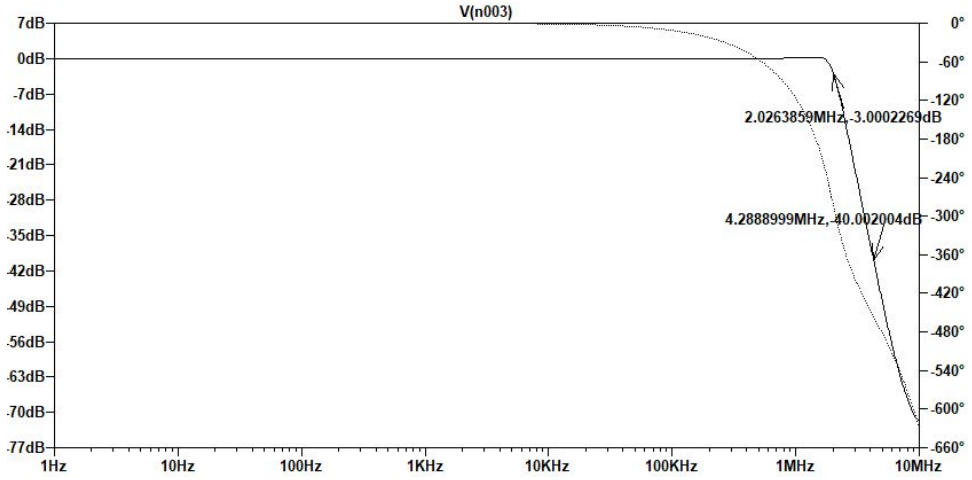

Figure 4.8: The AC response of the Filter

The filter is a 6th order butterworth filter with sallen-key topology at each stage. Figure 4.7 showed the schematic. The passband is up to 2MHz while the stopband is set at around 4.29MHz. Figure 4.8 shows where the bound of the passband and stopband are. The purpose of this filter is to filter unwanted noise that could influence the measurement result.

4.2.4 The transimpedance amplifier(TIA) and the programmable gain amplifier (PGA) combination

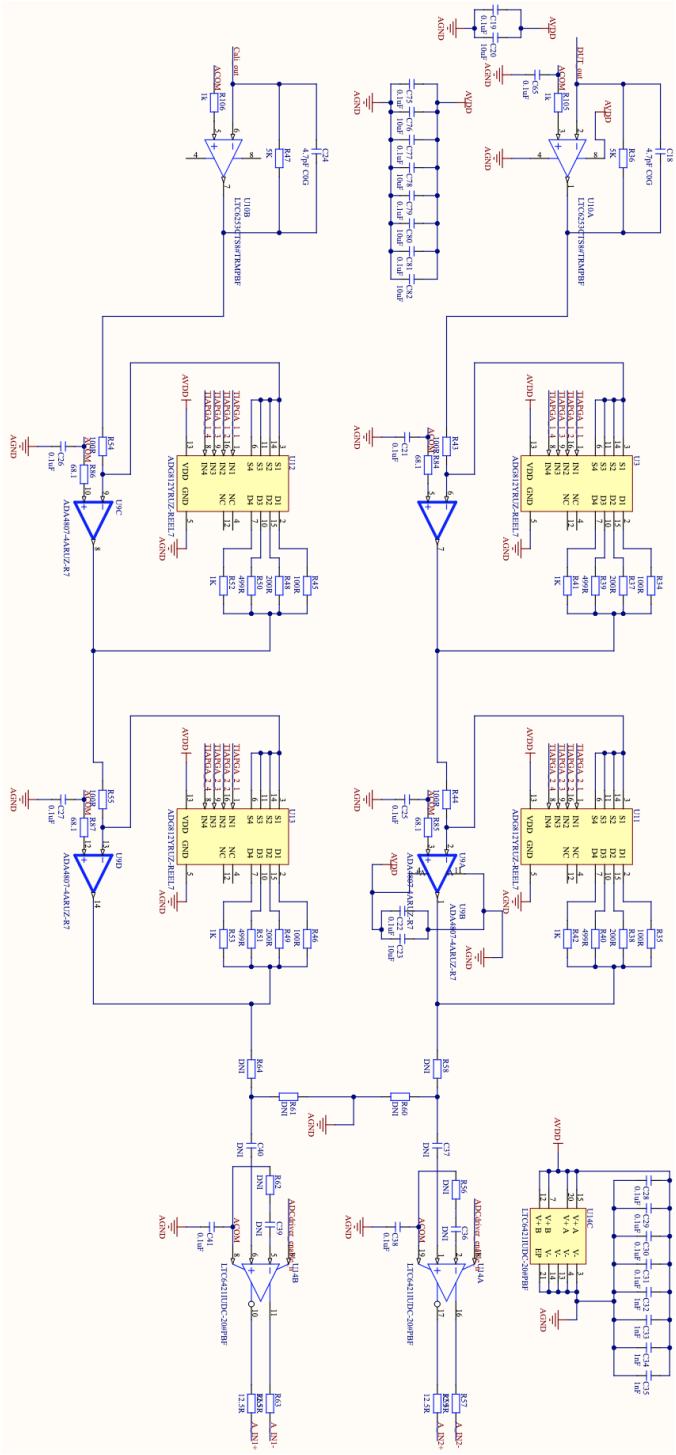

Figure 4.9: The schematic of the TIA and the PGA

As shown in the Figure 4.9, we have two sets of the TIA-PGA combination. We have the calibration resistor, and the device-under-test(DUT) goes in different paths. This time, we do not need to switch the signal between the calibration resistor and the DUT. The analog-digital-converter(ADC) is dual-channel so that we can collect the signals from different paths at the same time.

On each of the paths in the circuit, there are three stages. The first stage is the trans-impedance amplifier(TIA). And the following stages are the programable-gain-amplifiers.

We found that there is a factor that could lead to phase result inaccuracy in the impedance measuring. That is the phase response of the TIA. The function of the first step of the TIA is to convert a current signal to a voltage signal. We did not implement a current source in the design. The current is generated through the voltage applied over the sample test.

In Figure 4.9, DUT_out pin corresponds to the signal from the device-under-test, and the signal from the calibration resistor comes from the Cali_out pin. The magnitude of the impedance ranges from 1 kOhm to 100 kOhm. In order to couple with this value, we chose the value of R36 and R47 as 10 kOhm. C18 and C24 are the capacitor to extend the bandwidth.

Our aim is to maintain a phase accuracy within 1% at 1MHz testing frequency. In another word, when we change the value of the sample under test, the phase value should change inside 1%. In order to meet this demand, we need a good amplifier. After finding a lot of amplifiers with high Gain-Bandwidth, we chose LTC6253 amplifiers. The gain-bandwidth is 720MHz and it is a Rail-to-Rail amplifier, which means the swing of the signal can be higher. Compared to the ADA4807-4(GBW=180MHz) that were used in other blocks in the impedance board, the new one is more feasible in the design that requires a wide bandwidth. The result is that the phase response can be smoother around the frequencies that we are interested in.

Figure 4.10, 4.11 and 4.12 shows the simulation result when the DUT or calibration resistor's resistance is 1 kOhm, 10 kOhm, or 100kOhm, respectively.

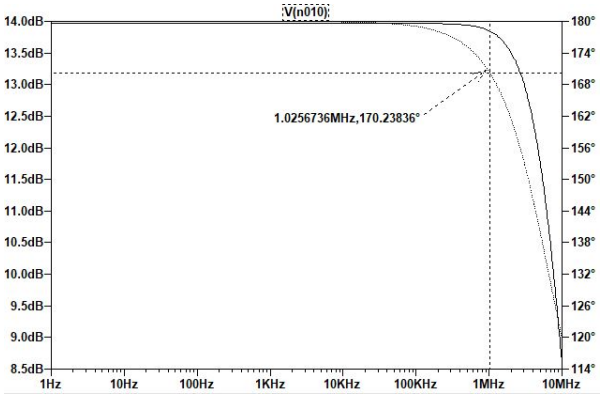

Figure 4.10: The simulation result when the sample's impedance or the calibration resistor is 1000.

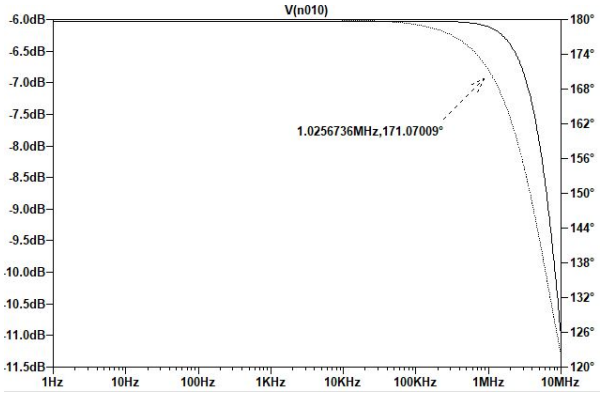

Figure 4.11: The simulation result when the sample's impedance or the calibration resistor is 10000.

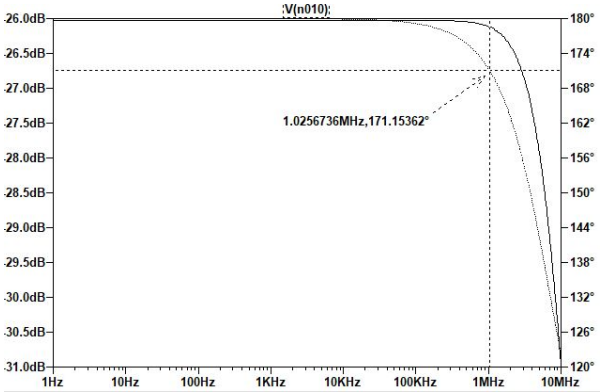

Figure 4.12: The simulation result when the sample's impedance or the calibration resistor is 100000.

4.2.5 The analog-digital converter (ADC) circuit

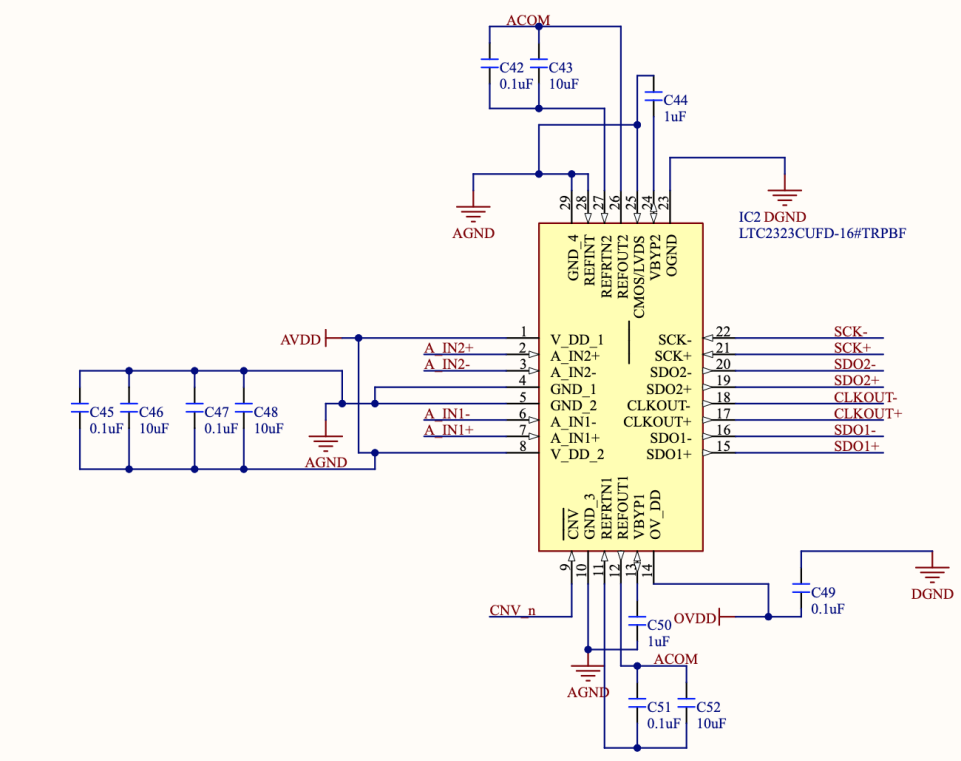

Figure 4.13: The schematic of the analog-digital converter(ADC) in the system

Figure 4.13 shows the ADC circuit that is with the LTC2323(Analog Device Inc.) ADC. This ADC is dual-channel to receive the signal from the calibration resistor and the DUT at the same time. We designed the pin configuration of the ADC by referring to the datasheet[102]. It is noticeable that the ADC requires a differential signal input. In Figure, two LTC6421 amplifiers transform the signal to a pair of differential signals so that the ADC can use them as input.

Also, there are pins connected to the FPGA. The FPGA control unit can send the control signal to the ADC and receive the digital signal from the ADC.

4.2.6 FPGA control unit

The FPGA is the control unit of the system. There are four different purposes for the FPGA control unit. Firstly, the FPGA needs to send control words

from the Direct Digital Synthesis(DDS) to the DAC. Then the DAC sends the sine signals to the rest of the analog front end(AFE). Also, the phase-lock-loop(PLL) in the system can guarantee the clock signal for the ADC, and the DDS are synchronized. Fast-Fourier-Transform(FFT) and the impedance calculation need to be performed on the FPGA chip. Finally, the data should be sent to a personal computer(PC) for display.

4.3 Testing result

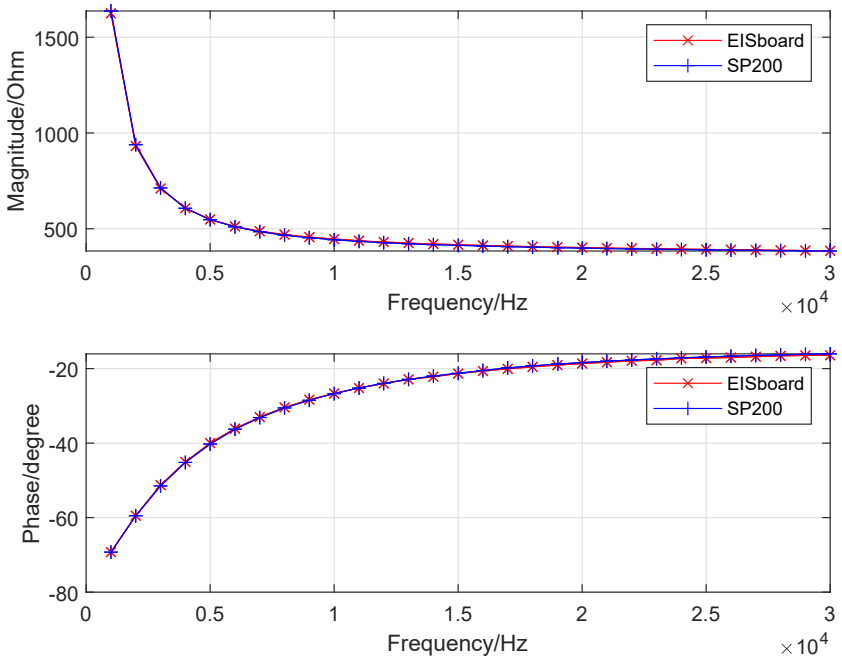

Figure 4.14: The testing result of the COVID-19 project impedance board

Figure 4.14 shows the comparison of the COVID-19 impedance board and the SP-200 when measuring a chip holder with no sample loaded, which is apparently a capacitive sample. The result shows a very good agreement between the results from the SP-200 and the impedance measurement system in the frequency range of sub-Hz to tens of kHz level.

4.4 Conclusion

This chapter only gives a brief introduction to the ongoing work: the COIVD-19 impedance measurement board. The author is responsible for the AFE design so that the AFE is mainly discussed. The test result shows that the system works well in a certain frequency range. Down the road, the impedance board is supposed to be work with real COVID-19 testing samples and try to help the diagnosis process.

Chapter 5

Conclusion

In this thesis, two different but similar work about the impedance measurement systems was introduced. For the corrosion impedance system, we introduced the background of the metal corrosion and the EIS analysis. Then we showed the hardware and software design of the corrosion impedance system. The system evaluation and the real corrosion experiment were conducted to show the system's performance. The result shows that our device has a good performance and can help to find insights into the corrosion phenomenon.

For the COVID-19 impedance measurement system, we introduced the background of the COVID-19 testing and its relationship with EIS analysis. Then we showed the design of the system and the testing result.

The thesis reflects the author's contribution to the development of the impedance measurement system.

References

[1] X. Hou, L. Gao, Z. Cui, and J. Yin, "Corrosion and protection of metal in the seawater desalination," in *IOP Conference Series: Earth and Environmental Science*, IOP Publishing, vol. 108, 2018, p. 022 037.

[2] D. C. Hansen, "Metal corrosion in the human body: The ultimate bio-corrosion scenario," *The Electrochemical Society Interface*, vol. 17, no. 2, p. 31, 2008.

[3] B. Wessling and J. Posdorfer, "Corrosion prevention with an organic metal (polyaniline): Corrosion test results," *Electrochimica Acta*, vol. 44, no. 12, pp. 2139–2147, 1999.

[4] A. El-Meligi, "Corrosion preventive strategies as a crucial need for decreasing environmental pollution and saving economics.," *Recent Patents on Corrosion Science*, 2010.

[5] A. A El-Meligi, "Corrosion of materials in polluted environment and effect on world economy," *Recent Patents on Corrosion Science*, vol. 1, no. 2, pp. 144–155, 2011.

[6] E. E. Stansbury and R. A. Buchanan, *Fundamentals of electrochemical corrosion*. ASM international, 2000.

[7] E. Schindelholz, B. Risteen, and R. Kelly, "Effect of relative humidity on corrosion of steel under sea salt aerosol proxies: I. nacl," *Journal of The Electrochemical Society*, vol. 161, no. 10, p. C450, 2014.

[8] X. Liu, J. Xiong, Y. Lv, and Y. Zuo, "Study on corrosion electrochemical behavior of several different coating systems by eis," *Progress in Organic Coatings*, vol. 64, no. 4, pp. 497–503, 2009.

[9] P. Li, T. Tan, and J. Y. Lee, "Corrosion protection of mild steel by electroactive polyaniline coatings," *Synthetic Metals*, vol. 88, no. 3, pp. 237–242, 1997.

[10] J. P. da Silva, S. C. De Torresi, and R. Torresi, "Polyaniline/poly (methylmethacrylate) blends for corrosion protection: The effect of passivating dopants on different metals," *Progress in organic coatings*, vol. 58, no. 1, pp. 33–39, 2007.

[11] N. Sato, "Basics of corrosion chemistry," *Green Corrosion Chemistry and Engineering*, vol. 1, 2012.

[12] G. Okamoto, M. Nagayama, J. Kato, and T. Baba, "Effect of organic inhibitors on the polarization characteristics of mild steel in acid solution," *Corrosion Science*, vol. 2, no. 1, pp. 21–27, 1962.

[13] J. Elze and H. Fischer, "The influence of inhibitors on the dissolution of iron in acid solution," *Journal of The Electrochemical Society*, vol. 99, no. 6, p. 259, 1952.

[14] M. G. Fontana and W. Stactile, "Corrosion science and technology," *Plenum Press, London*, vol. 1, p. 149, 1970.

[15] P. Pedeferri, "Cathodic protection and cathodic prevention," *Construction and building materials*, vol. 10, no. 5, pp. 391–402, 1996.

[16] S. C. Kolesar, "Principles of corrosion," in *12th International Reliability Physics Symposium*, IEEE, 1974, pp. 155–167.

[17] Z. Ahmad, *Principles of corrosion engineering and corrosion control*. Elsevier, 2006.

[18] V. Ashworth and C. J. Booker, "Cathodic protection: Theory and practice," 1986.

[19] L. Bertolini, F. Bolzoni, P. Pedeferri, L. Lazzari, and T. Pastore, "Cathodic protection and cathodic preventionin concrete: Principles and applications," *Journal of applied Electrochemistry*, vol. 28, no. 12, pp. 1321–1331, 1998.

[20] J. R. Macdonald and E. Barsoukov, "Impedance spectroscopy: Theory, experiment, and applications," *History*, vol. 1, no. 8, pp. 1–13, 2005.

[21] M. Carboni, J. Manzi, A. R. Armstrong, J. Billaud, S. Brutti, and R. Younesi, "Analysis of the solid electrolyte interphase on hard carbon electrodes in sodium-ion batteries," *ChemElectroChem*, vol. 6, no. 6, pp. 1745–1753, 2019.

[22] Y. Ko, Y.-G. Cho, and H.-K. Song, "Programming galvanostatic rates for fast-charging lithium ion batteries: A graphite case," *RSC Advances*, vol. 4, no. 32, pp. 16 545–16 550, 2014.

[23] I. Epelboin and M. Keddam, "Faradaic impedances: Diffusion impedance and reaction impedance," *Journal of the Electrochemical Society*, vol. 117, no. 8, p. 1052, 1970.

[24] I. Epelboin, P. Morel, and H. Takenouti, "Corrosion inhibition and hydrogen adsorption in the case of iron in a sulfuric aqueous medium," *Journal of the Electrochemical Society*, vol. 118, no. 8, p. 1282, 1971.

[25] I. Epelboin and M. Keddam, "Kinetics of formation of primary and secondary passivity in sulphuric aqueous media," *Electrochimica Acta*, vol. 17, no. 2, pp. 177–186, 1972.

[26] I. Epelboin, M. Keddam, and H. Takenouti, "Use of impedance measurements for the determination of the instant rate of metal corrosion," *Journal of Applied Electrochemistry*, vol. 2, no. 1, pp. 71–79, 1972.

[27] G. Makar and J. Kruger, "Corrosion studies of rapidly solidified magnesium alloys," *Journal of the Electrochemical Society*, vol. 137, no. 2, p. 414, 1990.

[28] K. Jüttner, "Electrochemical impedance spectroscopy (eis) of corrosion processes on inhomogeneous surfaces," *Electrochimica Acta*, vol. 35, no. 10, pp. 1501–1508, 1990.

[29] H. J. Habeeb, H. M. Luaibi, R. M. Dakhil, A. A. H. Kadhum, A. A. Al-Amiery, and T. S. Gaaz, "Development of new corrosion inhibitor tested on mild steel supported by electrochemical study," *Results in physics*, vol. 8, pp. 1260–1267, 2018.

[30] C. Cleveland, S. Moghaddam, and M. E. Orazem, "Nanometer-scale corrosion of copper in de-aerated deionized water," *Journal of The Electrochemical Society*, vol. 161, no. 3, p. C107, 2013.

[31] A. Velikonja, E. Gongadze, V. Kralj-Iglic, and A. Iglic, "Charge dependent capacitance of stern layer and capacitance of electrode/electrolyte interface," *Int. J. Electrochem. Sci*, vol. 9, no. 11, 2014.

[32] F. Nattino, M. Truscott, N. Marzari, and O. Andreussi, "Continuum models of the electrochemical diffuse layer in electronic-structure calculations," *The Journal of chemical physics*, vol. 150, no. 4, p. 041 722, 2019.

[33] S. M. M. Alavi, A. Mahdi, S. J. Payne, and D. A. Howey, "Identifiability of generalized randles circuit models," *IEEE Transactions on Control Systems Technology*, vol. 25, no. 6, pp. 2112–2120, 2016.

[34] R. N. Vyas, K. Li, and B. Wang, "Modifying randles circuit for analysis of polyoxometalate layer-by-layer films," *The Journal of Physical Chemistry B*, vol. 114, no. 48, pp. 15 818–15 824, 2010.

[35] X. Chen, Y. Shirai, M. Yanagida, and K. Miyano, "Effect of light and voltage on electrochemical impedance spectroscopy of perovskite solar cells: An empirical approach based on modified randles circuit," *The Journal of Physical Chemistry C*, vol. 123, no. 7, pp. 3968–3978, 2019.

[36] F. Mansfeld, C. Tsai, and H. Shih, "Software for simulation and analysis of electrochemical impedance spectroscopy (eis) data," in *Computer modeling in corrosion*, ASTM International, 1992.

[37] D. Ribeiro and J. Abrantes, "Application of electrochemical impedance spectroscopy (eis) to monitor the corrosion of reinforced concrete: A new approach," *Construction and Building Materials*, vol. 111, pp. 98–104, 2016.

[38] S. Grassini, S. Corbellini, M. Parvis, E. Angelini, and F. Zucchi, "A simple arduino-based eis system for in situ corrosion monitoring of metallic works of art," *Measurement*, vol. 114, pp. 508–514, 2018.

[39] G. Walter, "A review of impedance plot methods used for corrosion performance analysis of painted metals," *Corrosion Science*, vol. 26, no. 9, pp. 681–703, 1986.

[40] E. Angelini, D. Assante, S. Grassini, and M. Parvis, "Eis measurements for the assessment of the conservation state of metallic works of art," *Int. J. Circuits Syst. Signal Process*, vol. 8, pp. 240–245, 2014.

[41] T. Pajkossy, "Impedance spectroscopy at interfaces of metals and aqueous solutions — surface roughness, cpe and related issues," *Solid State Ionics*, vol. 176, no. 25, pp. 1997–2003, 2005, International Workshop on Impedance Spectroscopy for Characterisation of Materials and Structures, ISSN: 0167-2738. DOI: https://doi.org/10.1016/j.ssi.2004.06.023. [Online]. Available: https://www.sciencedirect.com/science/article/pii/S0167273805002031.

[42] M. Li, "Electrochemical impedance spectroscopy of tap water with the mfia (zurich instruments)," April 2, 2020.

[43] T. Ashworth, "Using the mfia impedance analyzer to characterize the esr of a super-capacitor (zurich instruments)," 1.11.2016.

[44] "Mfia 500 khz / 5 mhz impedance analyzer," https://www.zhinst.com.

[45] A. Yusof, K. Kalkandjiev, J. Schöndube, R. Zengerle, and P. Koltay, "Wafer level fabrication of an integrated microdispenser with electrical impedance detection for single-cell printing," *Proc. of Smart Systems Integration*, vol. 99, 2012.

[46] "Premium single channel potentiostat brochure," *www.biologic.net*,

[47] B. Jegdić, B. Bobić, B. Radojković, B. Alić, and L. Radovanović, "Corrosion resistance of welded joints of x5crni18-10 stainless steel," *Journal of Materials Processing Technology*, vol. 266, pp. 579–587, 2019.

[48] R. Pruna, F. Palacio, A. Baraket, N. Zine, A. Streklas, J. Bausells, A. Errachid, and M. López, "A low-cost and miniaturized potentiostat for sensing of biomolecular species such as tnf-α by electrochemical impedance spectroscopy," *Biosensors and Bioelectronics*, vol. 100, pp. 533–540, 2018.

[49] D. M. Jenkins, B. E. Lee, S. Jun, J. Reyes-De-Corcuera, and E. S. McLamore, "Abe-stat, a fully open-source and versatile wireless potentiostat project including electrochemical impedance spectroscopy," *Journal of The Electrochemical Society*, vol. 166, no. 9, B3056, 2019.

[50] N. Ebrahimi, M. Momeni, A. Kosari, M. Zakeri, and M. H. Moayed, "A comparative study of critical pitting temperature (cpt) of stainless steels by electrochemical impedance spectroscopy (eis), potentiodynamic and potentiostatic techniques," *Corrosion science*, vol. 59, pp. 96–102, 2012.

[51] X. Yu, M. Esanu, S. MacKay, J. Chen, M. Sawan, D. Wishart, and W. Hiebert, "An impedance detection circuit for applications in a portable biosensor system," in *2016 IEEE International Symposium on Circuits and Systems (ISCAS)*, IEEE, 2016, pp. 1518–1521.

[52] Z. Jiang, J. Yao, L. Wang, H. Wu, J. Huang, T. Zhao, and M. Takei, "Development of a portable electrochemical impedance spectroscopy system for bio-detection," *IEEE Sensors Journal*, vol. 19, no. 15, pp. 5979–5987, 2019.

[53] O. J. L. Gerasta, B. L. Barrientos, and C. M. Gerasta, "Impedance measuring device for metal solutions using a concave capacitive sensor," *IFAC-PapersOnLine*, vol. 51, no. 28, pp. 657–660, 2018.

[54] J. Punter-Villagrasa, B. del Moral-Zamora, J. Colomer-Farrarons, P. Miribel-Catala, I. Rodriguez-Villarreal, J. Cid, and B. Prieto-Simon, "Towards a portable point-of-use blood analysis with eis technique device," in *2014 IEEE 11th International Multi-Conference on Systems, Signals & Devices (SSD14)*, IEEE, 2014, pp. 1–6.

[55] J. Ferreira, F. Seoane, and K. Lindecrantz, "Portable bioimpedance monitor evaluation for continuous impedance measurements. towards wearable plethysmography applications," in *2013 35th Annual International Conference of the IEEE Engineering in Medicine and Biology Society (EMBC)*, IEEE, 2013, pp. 559–562.

[56] "Ad9834 functional block diagram," *www.analog.com*, 16/09/2020.

[57] "Pinout diagram of the arduino nano 33 ble," *www.arduino.cc*, 16/09/2020.

[58] K. R. Cooper, M. Smith, J. R. Scully, and N. D. Budiansky, "Development of a multielectrode array impedance analyzer for corrosion science and sensors," in *CORROSION 2006*, OnePetro, 2006.

[59] S. J. Ford, *Monitoring the corrosion of reinforcing steel in cement-based systems using impedance spectroscopy*. Northwestern University, 1998.

[60] M. Grossi and B. Riccò, "Electrical impedance spectroscopy (eis) for biological analysis and food characterization: A review," *Journal of sensors and sensor systems*, vol. 6, no. 2, pp. 303–325, 2017.

[61] W. Jung, *Op Amp applications handbook*. Newnes, 2005.

[62] S. Grassini, E. Angelini, M. Parvis, M. Bouchar, P. Dillmann, and D. Neff, "An in situ corrosion study of middle ages wrought iron bar chains in the amiens cathedral," *Applied Physics A*, vol. 113, no. 4, pp. 971–979, 2013.

[63] J. Hu, S.-a. Cao, and J. Xie, "Eis study on the corrosion behavior of rusted carbon steel in 3% nacl solution," *Anti-Corrosion Methods and Materials*, 2013.

[64] Y. Ma, Y. Li, and F. Wang, "Corrosion of low carbon steel in atmospheric environments of different chloride content," *Corrosion Science*, vol. 51, no. 5, pp. 997–1006, 2009.

[65] M. Mouanga, M. Puiggali, and O. Devos, "Eis and leis investigation of aging low carbon steel with zn–ni coating," *Electrochimica Acta*, vol. 106, pp. 82–90, 2013.

[66] M. A. Amin, S. S. Abd El-Rehim, E. El-Sherbini, and R. S. Bayoumi, "The inhibition of low carbon steel corrosion in hydrochloric acid solutions by succinic acid: Part i. weight loss, polarization, eis, pzc, edx and sem studies," *Electrochimica Acta*, vol. 52, no. 11, pp. 3588–3600, 2007.

[67] A. Benedeti, P. Sumodjo, K. Nobe, P. Cabot, and W. Proud, "Electrochemical studies of copper, copper-aluminium and copper-aluminium-silver alloys: Impedance results in 0.5 m nacl," *Electrochimica Acta*, vol. 40, no. 16, pp. 2657–2668, 1995.

[68] L.-G. ZHENG and H.-Y. YANG, "Influence of organic inhibitors on the corrosion behavior of steel rebar insidemortar specimens immersed in saturated nacl solution," *Acta Physico-Chimica Sinica*, vol. 26, no. 9, pp. 2354–2360, 2010.

[69] S. Zhao, Q. Lin, J. Ran, S. S. Musa, G. Yang, W. Wang, Y. Lou, D. Gao, L. Yang, D. He, *et al.*, "Preliminary estimation of the basic reproduction number of novel coronavirus (2019-ncov) in china, from 2019 to 2020: A data-driven analysis in the early phase of the outbreak," *International journal of infectious diseases*, vol. 92, pp. 214–217, 2020.

[70] T. P. Velavan and C. G. Meyer, "The covid-19 epidemic," *Tropical medicine & international health*, vol. 25, no. 3, p. 278, 2020.

[71] B. Pfefferbaum and C. S. North, "Mental health and the covid-19 pandemic," *New England Journal of Medicine*, vol. 383, no. 6, pp. 510–512, 2020.

[72] W. Cullen, G. Gulati, and B. Kelly, "Mental health in the covid-19 pandemic," *QJM: An International Journal of Medicine*, vol. 113, no. 5, pp. 311–312, 2020.

[73] K. Usher, J. Durkin, and N. Bhullar, "The covid-19 pandemic and mental health impacts," *International Journal of Mental Health Nursing*, vol. 29, no. 3, p. 315, 2020.

[74] P. K. Ozili and T. Arun, "Spillover of covid-19: Impact on the global economy," *Available at SSRN 3562570*, 2020.

[75] W. McKibbin and R. Fernando, "The economic impact of covid-19," *Economics in the Time of COVID-19*, vol. 45, 2020.

[76] L. L. Albu, C. I. Preda, R. Lupu, C. E. Dobrotă, G. M. Călin, and C. M. Boghicevici, "Estimates of dynamics of the covid-19 pandemic and of its impact on the economy," *Romanian Journal of Economic Forecasting*, vol. 23, no. 2, pp. 5–17, 2020.

[77] "Johns hopkins university medicine coronavirus resource center," coronavirus.jhu.edu/map.html,

[78] "Covid-19 info for albertans," www.alberta.ca,

[79] K. L. Schwartz, M. Murti, M. Finkelstein, J. A. Leis, A. Fitzgerald-Husek, L. Bourns, H. Meghani, A. Saunders, V. Allen, and B. Yaffe, "Lack of covid-19 transmission on an international flight," *Cmaj*, vol. 192, no. 15, E410–E410, 2020.

[80] A. Pal and M. Sankarasubbu, "Pay attention to the cough: Early diagnosis of covid-19 using interpretable symptoms embeddings with cough sound signal processing," in *Proceedings of the 36th Annual ACM Symposium on Applied Computing*, 2021, pp. 620–628.

[81] R. Chacón-Aguilar, J. M. Osorio-Cámara, I. Sanjurjo-Jimenez, C. González-González, J. López-Carnero, and B. Pérez-Moneo, "Covid-19: Fever syndrome and neurological symptoms in a neonate," in *Anales de pediatria*, Elsevier, 2020.

[82] R. T. Gandhi, J. B. Lynch, and C. Del Rio, "Mild or moderate covid-19," *New England Journal of Medicine*, vol. 383, no. 18, pp. 1757–1766, 2020.

[83] G.-u. Kim, M.-J. Kim, S. H. Ra, J. Lee, S. Bae, J. Jung, and S.-H. Kim, "Clinical characteristics of asymptomatic and symptomatic patients with mild covid-19," *Clinical microbiology and infection*, vol. 26, no. 7, 948–e1, 2020.

[84] J. Zhang, Z. Yang, X. Wang, J. Li, L. Dong, F. Wang, Y. Li, R. Wei, and J. Zhang, "The relationship between resilience, anxiety and depression among patients with mild symptoms of covid-19 in china: A cross-sectional study," *Journal of Clinical Nursing*, vol. 29, no. 21-22, pp. 4020–4029, 2020.

[85] H. Weerahandi, K. A. Hochman, E. Simon, C. Blaum, J. Chodosh, E. Duan, K. Garry, T. Kahan, S. L. Karmen-Tuohy, H. C. Karpel, *et al.*, "Post-discharge health status and symptoms in patients with severe covid-19," *Journal of general internal medicine*, vol. 36, no. 3, pp. 738–745, 2021.

[86] V. Jain and J.-M. Yuan, "Predictive symptoms and comorbidities for severe covid-19 and intensive care unit admission: A systematic review and meta-analysis," *International journal of public health*, vol. 65, pp. 533–546, 2020.

[87] C. P. West, V. M. Montori, and P. Sampathkumar, "Covid-19 testing: The threat of false-negative results," in *Mayo Clinic Proceedings*, Elsevier, vol. 95, 2020, p. 1127.

[88] J. Watson, P. F. Whiting, and J. E. Brush, "Interpreting a covid-19 test result," *Bmj*, vol. 369, 2020.

[89] J. Wu, J. Liu, S. Li, Z. Peng, Z. Xiao, X. Wang, R. Yan, and J. Luo, "Detection and analysis of nucleic acid in various biological samples of covid-19 patients," *Travel medicine and infectious disease*, vol. 37, p. 101 673, 2020.

[90] J. Zhifeng, A. Feng, and T. Li, "Consistency analysis of covid-19 nucleic acid tests and the changes of lung ct," *Journal of Clinical Virology*, vol. 127, p. 104 359, 2020.

[91] M. N. Esbin, O. N. Whitney, S. Chong, A. Maurer, X. Darzacq, and R. Tjian, "Overcoming the bottleneck to widespread testing: A rapid review of nucleic acid testing approaches for covid-19 detection," *Rna*, vol. 26, no. 7, pp. 771–783, 2020.

[92] M. J. Mulligan, K. E. Lyke, N. Kitchin, J. Absalon, A. Gurtman, S. Lockhart, K. Neuzil, V. Raabe, R. Bailey, K. A. Swanson, *et al.*, "Phase i/ii study of covid-19 rna vaccine bnt162b1 in adults," *Nature*, vol. 586, no. 7830, pp. 589–593, 2020.

[93] Y. Gao, L. Yan, Y. Huang, F. Liu, Y. Zhao, L. Cao, T. Wang, Q. Sun, Z. Ming, L. Zhang, *et al.*, "Structure of the rna-dependent rna polymerase from covid-19 virus," *Science*, vol. 368, no. 6492, pp. 779–782, 2020.

[94] T. K. Burki, "Testing for covid-19," *The Lancet Respiratory Medicine*, vol. 8, no. 7, e63–e64, 2020.

[95] D. Jacofsky, E. M. Jacofsky, and M. Jacofsky, "Understanding antibody testing for covid-19," *The Journal of arthroplasty*, vol. 35, no. 7, S74–S81, 2020.

[96] Z.-L. Liu, Y. Liu, L.-G. Wan, T.-X. Xiang, A.-P. Le, P. Liu, M. Peiris, L. L. Poon, and W. Zhang, "Antibody profiles in mild and severe cases of covid-19," *Clinical chemistry*, vol. 66, no. 8, pp. 1102–1104, 2020.

[97] J. Zhuang, J. Yin, S. Lv, B. Wang, and Y. Mu, "Advanced "lab-on-a-chip" to detect viruses–current challenges and future perspectives," *Biosensors and Bioelectronics*, p. 112 291, 2020.

[98] S. S. Mahshid, S. E. Flynn, and S. Mahshid, "The potential application of electrochemical biosensors in the covid-19 pandemic: A perspective on the rapid diagnostics of sars-cov-2," *Biosensors and Bioelectronics*, vol. 176, p. 112 905, 2021.

[99] J. Rodriguez-Manzano, K. Malpartida-Cardenas, N. Moser, I. Pennisi, M. Cavuto, L. Miglietta, A. Moniri, R. Penn, G. Satta, P. Randell, *et al.*, "Handheld point-of-care system for rapid detection of sars-cov-2 extracted rna in under 20 min," *ACS central science*, vol. 7, no. 2, pp. 307–317, 2021.

[100] M. Z. Rashed, J. A. Kopechek, M. C. Priddy, K. T. Hamorsky, K. E. Palmer, N. Mittal, J. Valdez, J. Flynn, and S. J. Williams, "Rapid detection of sars-cov-2 antibodies using electrochemical impedance-based detector," *Biosensors and Bioelectronics*, vol. 171, p. 112 709, 2021.

[101] "Ad9742 datasheet," www.analog.com,

[102] "Ltc2323 datasheet," www.analog.com,